

**SYNTHESIS OF SURFACE FUNCTIONALIZED  $\text{Cu}_2\text{O}$ ,  
 $\text{Au}@\text{Cu}_2\text{O}$  HYBRID FOR PHOTOCATALYTIC APPLICATION**

**BY**

**MOHAMMED TAJUDEEN ABDULLAHI**

A THESIS PRESENTED TO THE

DEANSHIP OF GRADUATE STUDIES

**KING FAHD UNIVERSITY OF PETROLEUM AND MINERALS**

DHAHRAN, SAUDI ARABIA

IN PARTIAL FULFILLMENT OF THE

Requirement for the Degree of

**MASTER OF SCIENCE**

**IN**

**CHEMISTRY DEPARTMENT**

**APRIL, 2020**

KING FAHD UNIVERSITY OF PETROLEUM & MINERALS

DHAHRAN- 31261, SAUDI ARABIA

**DEANSHIP OF GRADUATE STUDIES**

This thesis, written by **MOHAMMED TAJUDEEN ABDULLAHI** under the direction of his thesis advisor and approved by his thesis committee, has been presented and accepted by the Dean of Graduate Studies, in partial fulfillment of the requirements for the degree of **MASTER OF SCIENCE IN CHEMISTRY**.



Dr. **Muhammad Tahir Nawaz**  
(Advisor)



Dr. **Khalid R. Alhooshani**  
Department Chairman



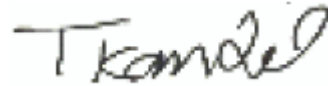
Dr. **Salam A. Zummo**  
Dean of Graduate Studies

12/5/2020

Date



PROFESSOR. **Nisar Ulah**  
(Member)



Dr. **Tarek Kandiel**  
(Member)



© MOHAMMED TAJUDEEN ABDULLAHI

2020

## **DEDICATION**

*To the glory my creator ALLAH Subhanahu Watahalah, THE ONE THE  
ETERNAL REFUGE, THAT IS NEITHER BEGETS NOR IS BORN,  
NOTHING IS EQUIVALENT TO HIM. Blessing to our prophet Muhammed  
(SAW) and my beloved parent*

## ACKNOWLEDGMENTS

My holistic superior thanks to my creator Almighty ALLAH for the gift of life and the grace to successfully achieve the great feat of completing my MS program in good health. May the peace and blessings of ALLAH be onto prophet MUHAMMAD (SAW), for given the world a child that floored the world with solution, contribute in making it a safe place for all, I ask ALLAH to increase HIS blessing and protection upon my both parent, my appreciation goes to my advisor, Dr. Muhammed Nawaz Tahir for his wisdom, coordination and supervision of my thesis title synthesis of surface functionalized  $\text{Cu}_2\text{O}$ ,  $\text{Au@Cu}_2\text{O}$  hybrid for photocatalytic application at the department of chemistry, KFUPM. I immensely draw from his load of experience on the best approach into research for academy excellence. My profound thanks is due to my thesis committee members, Professor Nisar Ulah for being so accommodative and fatherly guide, Dr. Tarek Kandiel for his open door relationship towards me, both for review of this work, advice on presentation skill and recommendation on the work in general.

I also like to thank the lab technician assistant for their numerous analysis support, particularly, Mr Hassan for SEM analysis. My sincere thanks to Prof. Dr. Basheer Chanbasha for allowing me to use his ultraviolet visible spectroscopy for the evaluation of the photocatalytic activity of the synthesized nanomaterial. The following are highly appreciated for guiding me through handling the following instruments, Mustapha Alhassan for XRD, Olabinton for Raman and Tauqir for UV-Vis spectroscopy.

Finally, I value the support of chemistry department through the chairman Prof. Dr. Khalid R. Alhooshani for providing resources use in the cause of my study and research work, my most valuable thank to the graduate coordinator Prof. Dr. Bassam ElAli for all favor and KFUPM for the offer of this great opportunity to earn a master degree through full scholarship.

|

## TABLE OF CONTENTS

DEDICATION.....	IV
ACKNOWLEDGMENTS .....	V
TABLE OF CONTENTS .....	VI
LIST OF TABLES .....	VIII
LIST OF FIGURES .....	IX
LIST OF ABBREVIATIONS .....	XII
ABSTRACT.....	XIII
ABSTRACT (ARABIC) .....	XIV
<b>1 CHAPTER 1 INTRODUCTION.....</b>	<b>1</b>
<b>1.1 Semiconductor Nanoparticle for Sunlight Harvesting .....</b>	<b>2</b>
<b>1.2 Hybrid Nanomaterial.....</b>	<b>3</b>
<b>1.2.1 Copper (1) Oxide Photoelectrochemistry uses .....</b>	<b>6</b>
<b>1.2.2 Noble Metal Nanoparticle .....</b>	<b>8</b>
<b>1.2.3 Semiconductor Nanoparticle.....</b>	<b>8</b>
<b>CHAPTER 2 LITERATURE REVIEW.....</b>	<b>11</b>
<b>2.1 The Development of Semiconductor Nanoparticle .....</b>	<b>11</b>
<b>2.1.1 Statement of Problem .....</b>	<b>17</b>
<b>2.1.2 Project Objectives .....</b>	<b>18</b>
<b>CHAPTER 3 RESEARCH METHODOLOGY.....</b>	<b>19</b>
<b>3.1 NANOMATERIAL SYNTHESIS .....</b>	<b>19</b>

3.1.1	Synthesis of Cu <sub>2</sub> O, Au@Cu <sub>2</sub> O Based Multi-Component Nanomaterials .....	19
3.1.2	Non-Aqueous Synthesis .....	19
3.1.3	Aqueous Synthesis.....	22
3.1.4	One Step Synthesis.....	22
3.1.5	Two Step Synthesis .....	24
3.1.6	Synthesis of Au@Cu <sub>2</sub> O Hybrid Nanoparticles.....	25
3.1.7	Characterization of Multi-Component Nanoparticles .....	27
<b>CHAPTER4 RESULTS AND DISCUSSIONS .....</b>		<b>28</b>
4.1	Spectroscopy Characterization.....	28
4.2	Scanning Electron Spectroscopy (SEM) Image .....	29
4.3	Energy-dispersive X-ray (EDX) Spectroscopy .....	38
4.4	Ultraviolet-Visible (UV-Vis) Spectroscopy .....	42
4.5	RAMAN Spectroscopy.....	46
4.6	X-ray Diffraction (XRD) .....	47
4.7	Photocatalytic Application .....	52
<b>CHAPTER 5 CONCLUSION AND RECOMMENDATIONS .....</b>		<b>58</b>
<b>REFERENCES.....</b>		<b>61</b>
<b>VITAE.....</b>		<b>65</b>

## LIST OF TABLES

<b>Table 1</b> , Shows the Theoretically Calculated, Mass Ratio of Cu and O in Cu <sub>2</sub> O and the Au, Cu, And O in Au@Cu <sub>2</sub> O.....	34
---	----

## LIST OF FIGURES

Figure 1 I-V Curve of Photovoltaic (PV) in Darkness & Illumination.....	3
Figure 2 Gold is Yellow Dots and Wine Color Represent Copper (1) Oxide.....	3
Figure 3 Cube Au@Cu <sub>2</sub> O & Octahedron Au@Cu <sub>2</sub> O in A Shell-Core Hybrid.....	6
Figure 4 Crystallography Representation of Cu <sub>2</sub> O, Copper in Orange And Oxygen in Red Color.....	8
Figure 5 UV-Vis Spectra of Non-Aqueous Synthesized Cu <sub>2</sub> O.....	9
Figure 6 SEM Image of the Cu <sub>2</sub> O, Synthesized with Sodium Dodecyl Sulfate (SDS) a Surfactant.....	31
Figure 7 Bears the SEM Image of Cu <sub>2</sub> O Synthesized with Limited Addition of SDS.....	32
Figure 8 SEM Image of Cu <sub>2</sub> O with All Reaction Condition Maintained.....	33
Figure 9 SEM Image of Cu <sub>2</sub> O Nanoparticle Synthesized with Long Growth Time.....	34
Figure 10 SEM Image of Cu <sub>2</sub> O, Decorated with Au Nanoparticle.....	35
Figure 11 SEM Image of Octahedron Cu <sub>2</sub> O Nanoparticle.....	36
Figure 12 SEM image of Octahedron Cu <sub>2</sub> O with Au decoration.....	37
Figure 13 SEM Image of Pristine Octahedron Cu <sub>2</sub> O with Au Nanoparticle.....	38
Figure 14 EDX of Cube Shaped Cu <sub>2</sub> O.....	39
Figure 15 EDX Mapping of Cubed Shaped Au@Cu <sub>2</sub> O.....	40
Figure 16 EDX Mapping of Octahedron Au@Cu <sub>2</sub> O.....	41
Figure 17 UV-Vis Spectra of Cubed Shaped Cu <sub>2</sub> O .....	43
Figure 18 Kinetic UV-Vis Spectra of Au@Cu <sub>2</sub> O .....	44
Figure 19 UV-Vis Spectra of Octahedron Cu <sub>2</sub> O .....	45
Figure 20 Raman Shift Pattern of Cube Shaped Cu <sub>2</sub> O & Au@Cu <sub>2</sub> O.....	46
Figure 21 Raman Band of Octahedron Cu <sub>2</sub> O Nanoparticle.....	47

Figure 22 XRD Diffractogram of Cu <sub>2</sub> O without & with SDS.....	48
Figure 23 XRD Diffractogram of Au@Cu <sub>2</sub> O.....	49
Figure 24 XRD Diffractogram of Octahedron Shaped Cu <sub>2</sub> O.....	50
Figure 25 XRD Diffractogram of Octahedron Shaped Au@Cu <sub>2</sub> O.....	51
Figure 26 Photo-Degradation of ME Activity of Cube Shaped Cu <sub>2</sub> O.....	54
Figure 27 Au@Cu <sub>2</sub> O Hybrid Photo-Degradation of M.....	55
Figure 28 MB Degradation by Octahedron Cu <sub>2</sub> O.....	56
Figure 29 Octahedron Au Decorated Cu <sub>2</sub> O Photo-Degradation of MB.....	57
Figure 30 Photocatalytic Degradation Kinetics of Methylene Blue.....	58

## LIST OF SCHEMES

Scheme 1 Cu <sub>2</sub> O Schell with Au Cure .....	13
Scheme 2 Au@Cu <sub>2</sub> O Photocatalytic Effect.....	13
Scheme 3 Photoelectrochemical Cell Operation Using N-Type Semiconductor.....	15
Scheme 4 Bottom-Up Synthesis of Nanoparticle.....	22
Scheme 5 Synthesis Pathway of Cube and Octahedron Cu <sub>2</sub> O.....	23
Scheme 6 Cube Morphology Cu <sub>2</sub> O Nanoparticle.....	25
Scheme 7 Cube Shaped Cu <sub>2</sub> O, Decorated Au.....	25
Scheme 8 Synthesis of Heterodimer and Multimers Au@Cu <sub>2</sub> O .....	26
Scheme 9 Synthesis Step and Color Changes.....	29
Scheme 10 Presented the Band Gap of Cu <sub>2</sub> O.....	53

## LIST OF ABBREVIATIONS

<b>EDX</b>	:	Electron Diffraction X-Ray Spectroscopy
<b>SEM</b>	:	Scanning Electron Microscopy
<b>SDS</b>		Sodium Dodecyl Sulfate
<b>MB</b>		Methylene Blue

## ABSTRACT

Full Name : MOHAMMED TAJUDEEN ABDULLAHI  
Thesis Title : SYNTHESIS OF SURFACE FUNCTIONALIZED  $\text{Cu}_2\text{O}$   $\text{Au}@\text{Cu}_2\text{O}$   
HYBRID FOR PHOTOCATALYTIC APPLICATION  
Major Field : Chemistry  
Date of Degree : April, 2020

The environmental concern raised due to the use of conventional fuel for energy production which results in increasing the level of  $\text{CO}_2$  and to remediate industrial dumped organic pollutants especially dyes into the ocean body, demands for alternatives renewable energy resources. There is an increasing need to develop new materials or improve the existing options to exploit the available carbon neutral energy resources such as hydrogen fuel using photo-electrochemical (PEC) water splitting or degradation of pollutants using solar light. The both processes require the design and synthesis of new materials which are cost effective, environmentally friendly, capable of harvesting maximum range of the solar spectrum, electrically and chemically stable, with suitable band-edge potentials to perform the function. In this project we accomplished the synthesis of pristine  $\text{Cu}_2\text{O}$  nanoparticles consisting and hybrid nanomaterial with the composition Au and  $\text{Cu}_2\text{O}$ . Due to the low band gap  $\sim 2.1$  eV of  $\text{Cu}_2\text{O}$  and its suitable conduction band edge positions, it is among the most favorite semiconductors available for visible light base photocatalytic applications. The hybridization of Au and  $\text{Cu}_2\text{O}$  improved the solar absorption efficiency, photocatalytic activity and the chemical stability of these materials under working conditions.

## ABSTRACT (ARABIC)

الكامل الاسم: MOHAMED TAJUDEEN ABDULLAHI

الضوئي التحفيز لتطبيق Cu<sub>2</sub>O @ Hybrid Au و Cu<sub>2</sub>O وتوصيف تحضير: الرسالة عنوان

كيمياء: الدقيق التخصص

الدرجة تاريخ: أبريل 2020

العضوية الصبغة ومعالجة الكربون أكسيد ثاني مستوى زيادة مع للتعامل أخرى مناطق في فعالة بيئية بإدارة الاهتمام الكربون المحايدة الطاقة موارد لإنتاج المواد تحسين / لتطوير متزايدة حاجة هناك ، المحيط جسم في الملقاة الصناعية الضوئي للتحلل ضوئي وحفز المياه لتقسيم (PEC) الكهروكيميائية المواد- الصور باستخدام الهيدروجين وقود مثل أقصى حصاد على القدرة الجديدة للمواد التكلفة حيث من الفعالين والتركيب التصميم فإن ، لذلك .العضوية للصبغة مفر لا أمر المياه لتقسيم المناسبة النطاق حافة إمكانات مع ، وكيميائيًا كهربائيًا المستقر ، الشمسي الطيف من مدى مع الهجينة النانوية والمواد ، O و Cu من يتكون مركب أصلي نانوي جزيء بإنجاز قمنا ، المشروع هذا في .منه فجوة بسبب ، العمل ظروف في المواد لهذه الكيميائي الاستقرار لتحسين السطح وهندسة Cu<sub>2</sub>O و Au التركيبي المفضلة الموصلات أشباه بين من وهي ، المناسبة التوصيل حافة مواضع و Cu<sub>2</sub>O - 2.1 eV ~ المنخفض النطاق المرئية الضوء لقاعدة الضوئي التحفيز لتطبيقات المتاحة.

# CHAPTER 1

## INTRODUCTION

The advancement in technology is in the forefront of developmental strive of modern era with energy being very important necessity for driving this race. Therefore, there is an ever increasing demand for energy both in the developed and developing countries. Human well-being is much related to the access to energy, due to its impact on economic development and reducing the poverty. The hardcore challenge that threatens the world development is how to ensure everyone has access to the sufficient amount of energy and safe clean water for their optimum functioning. Although, the present sources of energy like coal, gas and crude oil pose a great environmental concern to the world, still fossil fuels (oil, gas and coal) have dominated our energy sources over the years. It produces atmospheric pollutants with devastating foot prints of different degree in every part of the world. To reverse this trend, it is paramount to transit from fossil fuel based source of energy to renewable energy resource *i.e.* bioenergy, wind, hydropower and solar energy. The renewable resources have a huge potential as a source of energy with no or little environmental damage<sup>1</sup>.

Among the renewable sources available, solar power exposing  $1.2 \times 10^{14}$  kJ/sec of energy to Earth's surface is the most promising option<sup>2</sup>. The efficient conversion of solar power using renewable resources such as photo-electrochemical (PEC) water splitting to produce hydrogen fuel could be the cost effective and environmentally friendly alternatives to meet world energy demands. The solar spectrum could successfully provide the required energy ( $286 \text{ kJ mol}^{-1}$ ) input to split water at room temperature and pressure<sup>3</sup>. Therefore,

the design and synthesis of new functional materials capable of; **(i)** harvesting the maximum range of solar spectrum, **(ii)** electrically and chemically stable and **(iii)** with suitable band-edge potentials to split water are inevitable.

The advances towards tapping into visible light photoactive semiconductors has seen interest even in non-oxide based photocatalyst such as (oxy)nitride (e.g.  $C_3N_4$  and  $TaON_4$ ), also sulphide like  $MoS_4$ ,  $CuInS_2$  and  $CdS$  semiconductors<sup>5</sup>. However, the narrow band gap of the mentioned photocatalyst contributed to their relatively weak reduction, that is a low negative conduction band (CB) and/or oxidation which implies a low positive valence band (VB) potentials. So there is a need to develop the materials with a suitable band gap as well as positions of valence and conduction band. The  $Cu_2O$  fulfills the necessary criteria required for  $H_2$  production using solar light. Cuprous oxide ( $Cu_2O$ ) has a band gap of 2.0-2.4 eV suitable for water redox reaction and an excellent material for photocatalytic organic dye degradation<sup>6</sup>.

## 1.1 Semiconductor Nanoparticle for Sunlight Harvesting

The mindset on how to harvest the solar power for valuable uses in electricity or to bring about chemical reaction has been around with us since the discovery of the possibility of generating electricity upon exposure of semiconductor material to sunlight. Civilization comes with a huge price, as the energy harness to meet increasing needs of energy by consumers on their pursuit for civilization and to attain comfort. Developing nations at present drive for technology are consuming energy at an unprecedented rate. This energy, is majorly produced using fossil resources. Earlier human relies on his own power to perform a task, but industrial boom facilitated invention of machines that now do those task human has done earlier and these machines run on fossil fuel directly or indirectly.

The unending race of civilization is threatening our present finite energy sources and soon we might run out of oil, scarcity will set in and energy from fossil fuel will no longer be available or affordable to us. Presently, our civilization energy up take is about 18TW ( $18 \times 10^{12} \text{ W}$ )<sup>7</sup>, and it is expected to be more than double the rate in nearest future<sup>8</sup>.

The solar energy with capacity to expose light on earth which can produce  $3.846 \times 10^{26} \text{ W}$  of energy per second could be the potential alternative energy generation option to maintain the demands of world energy. However, to do so, we need suitable of light absorbing materials. The inorganic based semiconductor has shown great potential. The energy when captured by semiconductor is converted to electricity through photovoltaics effect, (Figure 1), as a model where the source of current parallel with a diode and as the light intensity increases so is the current generated by the photovoltaic (PV) cell. In the absent of light, the PV act as a diode<sup>9</sup>.

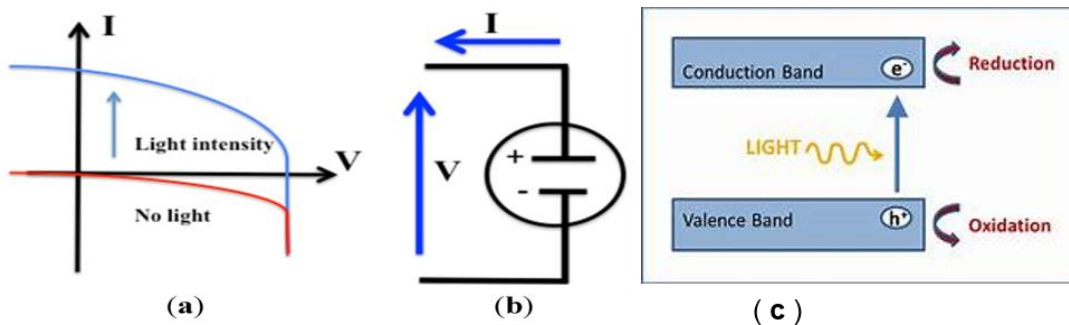


**Figure 1**, (a) I-V Curve of photovoltaic (PV) cell in darkness and under illumination; (b) Electrical diagram of a PV cell; (c) Semiconductor light induced redox reaction

## 1.2 Hybrid Nanomaterial

These are composites materials which consist of more than one constituents, connected to each other in the nanometer size regime at the same platform. It could be

a combination of inorganic semiconductors such as  $\text{TiO}_2$ ,  $\text{Cu}_2\text{O}$ ,  $\text{Fe}_2\text{O}_3$ ,  $\text{MnO}$  based nanomaterial joined with plasmonic metal like Au, Ag, or Cu on the surface of the use inorganic semiconductors. These materials not only present the combined properties of individual constituents but also new properties of the hybrid as a result of electronic communication between the different domains.<sup>10</sup> There is a decrease in the electromagnetic frequency of a semiconductor when plasmonic metal were introduced into its surface, and given that there is an inverse relation between frequency and wavelength, therefore,  $\text{MNO}$  with Au hybrid interaction will lead to a red shift in the absorption of electromagnetic radiation by the hybrid nanomaterial. The size of noble metal domain has a huge contribution to the overall new effect exhibited by the newly formed hybrid materials. For instance, a pure Au nanoparticle with 5-20 nm size range shows a collective plasmon resonance which correspond to 520-525 nm, and this was red shifted to 555-585 nm when the Au nanoparticle was attached  $\text{Cu}_2\text{O}$ <sup>11</sup>. Figure 2, shows a hybrid nanomaterial consisting of Au metal domain (in yellow color) and  $\text{Cu}_2\text{O}$  semiconductor component (wine color). This combination ensures a cheap hybrid nanomaterial consisting largely of efficient, less toxic and abundantly available materials. The architecture of the hybrid material also enables the metal to contribute maximum for charge separation.

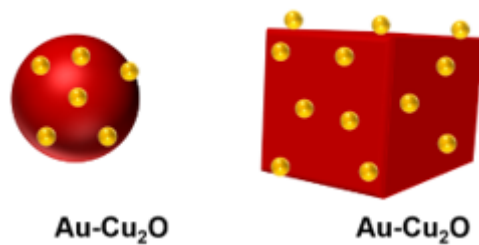


**Figure 2**, Gold is the yellow dots and wine color represent copper (1) oxide

Metal oxide semiconductor photocatalyst has been proven to be highly desirable for several applications. Basically, ultraviolet (UV) light absorbing semiconductors with wide band gap are usually employed as photocatalytically active materials<sup>11</sup>. The semiconductor materials such as TiO<sub>2</sub><sup>12</sup>, ZnO<sup>13</sup>, among others has gain great attention due to UV light harvesting properties where as CdS<sup>14</sup> is the best visible light harvesting semiconductor. In the face of this remarkable usefulness of these metal oxides semiconductors, there are many shortcomings which hampers their function to be used as efficient photocatalysts. These are still matter of concerns for their use as semiconductor material at large scale. The noticed shortcomings are faster charge carrier recombination, low stability in recycling and low photo induced reaction efficiency. This warrant the need to study the photocatalytic performance of cuprous oxide to add to the recent effort by the scientists on this semiconductor material<sup>15,16,17</sup>. Figure 3, represent the scheme with noble metal as core and Cu<sub>2</sub>O as shell materials. This design is among the already well established metal-semiconductor based nanoparticles. However, noble metal being inside as core cannot contribute for charge separation, one of the key parameter which defines the best efficiency of the photocatalyst.

Cu<sub>2</sub>O is well known for its well-placed conduction band (CB) and valence band (VB) for the overall oxidation of water splitting<sup>18</sup>. Typically, semiconductor is either that with direct band gap or indirect band gap, but Cu<sub>2</sub>O is a good example of direct band gap semiconductor. A band gap is the minimum energy difference that is between the valence band (VB) at the top and the conduction band (CB) at the bottom. The electron momentum at the bands are usually not of the same values. The Energy maxima in the valence band

and the energy minima in the conduction band are define by certain crystal momentum and  $k$ -vector (propagation constant) in the Brillouin zone. Basically,  $\text{Cu}_2\text{O}$  conduction band minima and valence band maxima,  $k$ -vector are the same which imply a direct band gap semiconductor. In a direct band gap, the momentum of electrons & holes is similar for both the conduction band and the valence band, this electron can emit photon. The direct band semiconductor electron in conductor band (CB) minima, recombine directly with holes in valence band (VB) maxima without change in kinetic energy and momentum, where energy in the form of light is spontaneous emission<sup>19</sup>.

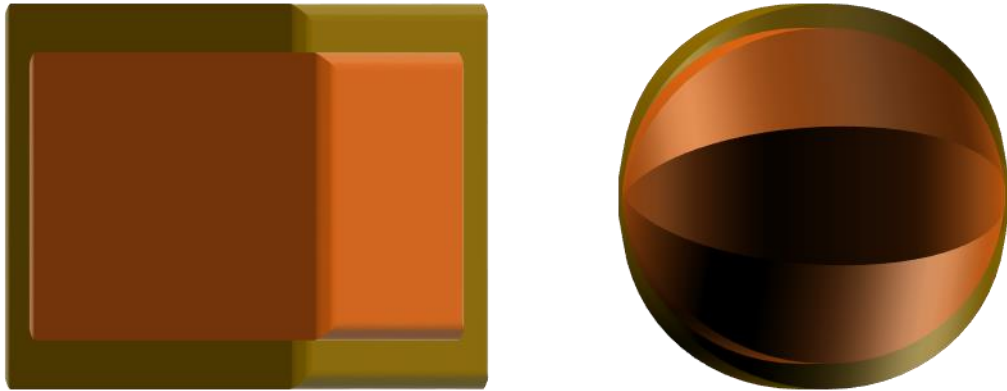


**Figure 3**, Cube  $\text{Au@Cu}_2\text{O}$  & Octahedron  $\text{Au@Cu}_2\text{O}$  in a gold shell-copper oxide core hybrid nanomaterial

### 1.2.1 Copper (I) Oxide Photoelectrochemistry uses

Photoelectrochemical production of hydrogen through the splitting of water from the direct harvesting of solar energy using semiconductor can ease the issue of energy conservation and storage associated with solar electricity production. The associated cost with the existing methods give PEC an edge as a promising innovative technique for ultimate solar fuel generation, in this case hydrogen<sup>20</sup>. The stability and efficiency of the

system also count in determining the best choice for the water splitting method. The efficiency of solar to hydrogen (STH) water splitting system can be define as

$$STH = \left( \frac{J_{Photo} [mA/cm^2] \times 1.23V \times \eta_F}{Power [mW/cm^2]} \right) \quad 1$$

Where the symbol  $J_{Photo}$  is the photocurrent density per geometric area and  $\eta_F$  stand for the faradiac efficiency for hydrogen evolution. This equation is useful when sacrificial agents like methanol are not used and oxygen evolution occurs<sup>20</sup>.

The value 1.23V is the reversible voltage needed for water splitting and represents the highest electrical energy that can be harvested by reacting hydrogen and oxygen to produce liquid water in a fuel cell<sup>21</sup>.

Therefore, in this project we would accomplish the synthesis of plasmonic metals (Au) and low bandgap semiconductor ( $Cu_2O$ ) based hybrid nanoparticles using bottom up wet chemical approaches to solve the both impairments related to its use as photocatalytic applications. The strategy will focus to engineer the  $Cu_2O$  domain; **(a)** by controlling the size and shape of  $Cu_2O$  domain in the nano-regime and improving the photostability of the  $Cu_2O$  domain by combining with plasmonic mateals<sup>22,23</sup>. The wet chemical synthesis gives the best opportunity to control the nucleation and growth steps by controlling heating rate/temperature, employing proper solvents and stabilizing ligands. This strategy will help stabilizing the  $Cu_2O$  domains in the nano-regime by compensating the surface energy through proper ligand binding<sup>24</sup>.

## 1.2.2 Noble Metal Nanoparticle

Surface plasmon resonance (SPR) is very well associated with noble metal nanoparticles (NPs) due to the behavior of their free surface electrons that oscillate with the same frequency of the incident electromagnetic radiation<sup>25</sup>. Noble metal nanoparticles are unique in their capacity to exhibit local surface plasmon resonance (LSPR) optical properties. The presence of resonating plasmon is attributed to the loads of free electrons and stabilities in chemical environment as seen in the case of gold (Au) and Silver (Ag) nanoparticle. These nanoparticles are being exploited for the plasmonic field applications because of its large LSPR support for wide region of the electromagnetic radiation spectrum. However, the LSPR of Ag nanoparticle has a stronger intensity than observed in other noble metals, perhaps, its low refractive index could account for this performance in case of silver<sup>26,27</sup>. However, the chemical stability of silver is compromised under working condition. The ease of fabrication of Au nanoparticles along with its high chemical stability prompted their use as a plasmonic metal nanoparticle much more than any other metal based materials such as Ag and Cu. The noble metal based nanoparticles have also considerably gained attention as a sensor<sup>28</sup>. Biological/Chemical sensor usefulness of a nanomaterial is determined by the refractive index sensitivity of nanoparticles.

## 1.2.3 Semiconductor Nanoparticle

Metal oxides have gained tremendous use as a semiconductor such as TiO<sub>2</sub>, WO<sub>3</sub>, and CuO due to their ability to harvest sunlight. They could be categorized as either p-type or n-type depending on their conduction band and valence band position. Among which copper oxide is a p-type semiconductor with wide distribution on the earth, relatively cheap and non-toxic transitional metal oxide. It can exist in various forms such as Cu<sub>4</sub>O<sub>3</sub>, CuO

and  $\text{Cu}_2\text{O}$ <sup>29</sup>. The first two is less commonly used in such applications compare to  $\text{Cu}_2\text{O}$ . Figure 4, shows the crystal structure of  $\text{Cu}_2\text{O}$  (Cubic Bravais lattice), with the space group  $\text{Pn}\bar{3}\text{m}$  (224) and has a lattice constant of  $4.2696 \pm 0.0010 \text{ \AA}$ <sup>30</sup>. Copper atom is coordinated to two oxygen linearly and oxygen atoms which occupies the body center and the edge of the cubic unit cell, individually coordinated to four copper atoms in a tetragonal fashion.

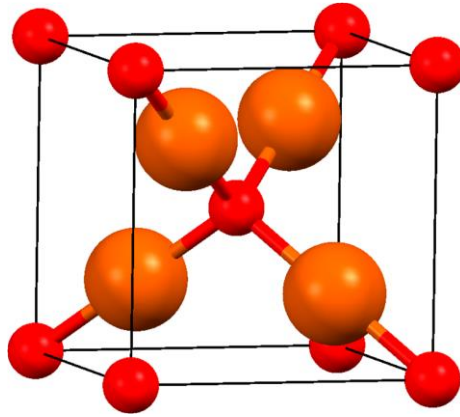


**Figure 4**, shows the crystal structure of  $\text{Cu}_2\text{O}$  (Cubic Bravais lattice), with the space group  $\text{Pn}\bar{3}\text{m}$  (224) and has a lattice constant of  $4.2696 \pm 0.0010 \text{ \AA}$ . Copper in orange and oxygen in red color.

Furthermore, the valence band gap and the conduction band are presented in Figure 5, Cu  $d^{10}$  orbitals constitute the upper valence band and the s-orbital like character constitute the lower conduction band, which is the Cu 4s orbitals<sup>31</sup>. Interestingly, the allowed transition is ( $\Gamma_8^+ \longrightarrow \Gamma_8^-$  and  $\Gamma_7^+ \longrightarrow \Gamma_8^-$ ) and the absorption transitions ( $\Gamma_8^+ \longrightarrow \Gamma_6^+$  and  $\Gamma_7^+ \longrightarrow \Gamma_6^+$ ) are forbidden in nature. The allow transition resulted in the much higher absorption coefficients at their corresponding wavelengths. The forbidden nature of the

lower energy direct transition of  $\text{Cu}_2\text{O}$  makes it behaves more like an indirect semiconductor even though it is a direct semiconductor<sup>32</sup>.

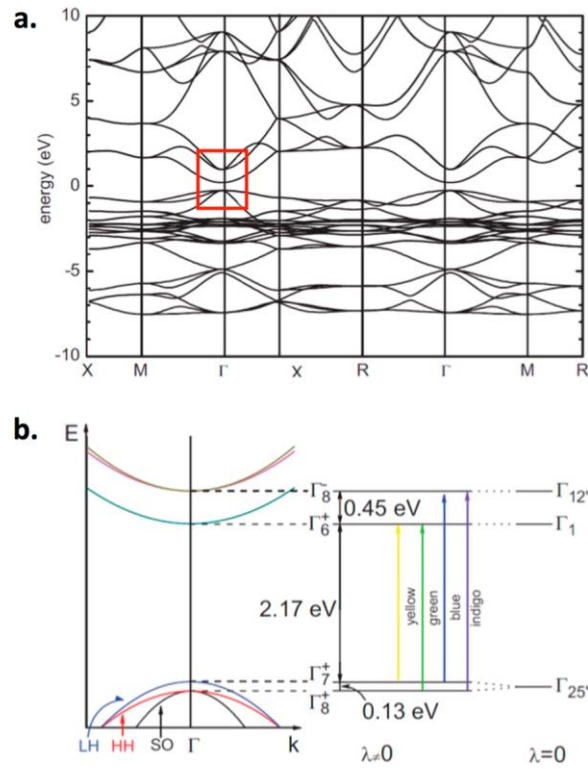


**Figure 5,** (a) Estimated band structure of  $\text{Cu}_2\text{O}$ . (b) A view on bandgap highlighted in red in (a)<sup>30</sup>

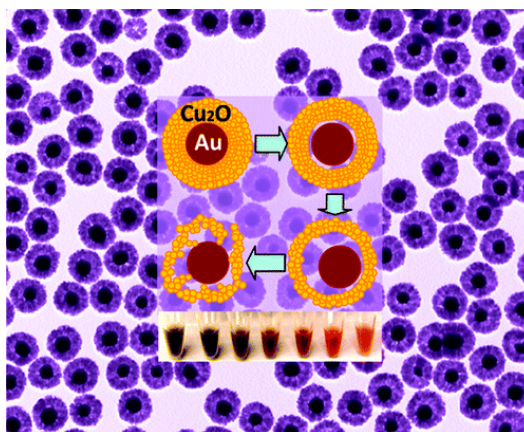
## [ CHAPTER 2 ]

### [ LITERATURE REVIEW ]

#### 2.1 The Development of Semiconductor Nanoparticle

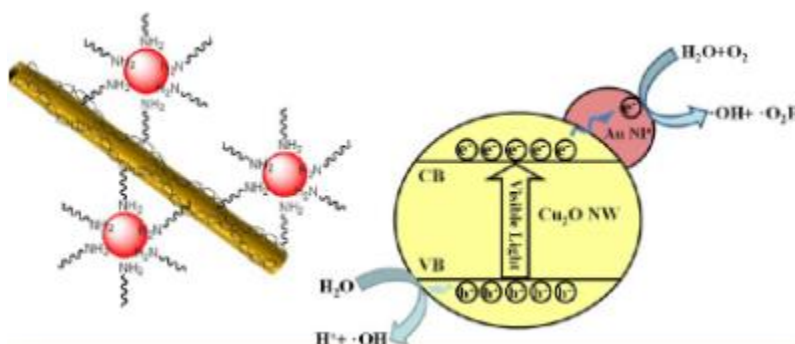
The solution synthesized nano-gold-copper oxide of specific dimension showed very high electronic properties with an optimized photocatalytic viability<sup>33</sup>. Varying the concentration of the reducing agent present in the reaction, nucleation of the expected product takes different forms with promising facet present on the surface, that significantly determine the electro-optical properties of the pristine Cu<sub>2</sub>O semiconductor target nanotube<sup>33</sup>. Addition of metal as core nanocrystal further pushed the electrical conductivity and optical properties of gold-copper oxide for better solar energy utilization. In their work, Kuo et al., showed the facet dependent photocatalytic properties of the synthesized Cu<sub>2</sub>O nanoparticles. The pure Cu<sub>2</sub>O nanoparticles with octahedral morphology and bounded by {111} facets were 1100 times more conductive compared to the pure Cu<sub>2</sub>O having cube shape and crystal bounded by {100} facets. The Cu<sub>2</sub>O nanoparticles when hybridized with Au core, showed the enhanced, electrical and photocatalytic properties<sup>34</sup>. It is possible to achieve Au nanoparticles with octahedral geometry and this concentrated nano-shape gold crystal were used as seed crystals to grow Au/Cu<sub>2</sub>O hybrid. The conductivity of these hybrid nanoparticles became 10,000 fold more than pure Au octahedra<sup>35</sup>. The work also showed how the photodegradation of organic pollutant using Au-Cu<sub>2</sub>O core shell heterostructure outperformed the pristine Cu<sub>2</sub>O nanoparticles. The improved photocatalytic performance was attributed to the efficient photoinduced charge separation due to metal and metal oxide interfacial electronic communication<sup>36</sup>.

The photothermal activities for the photodegradation of organic pollutant and water splitting of core-shell noble metal-semiconductor nanocubes, octahedral and nanobars were also reported. Wang et al, Reported, Scheme 1, the facet dependent heat production properties of Au-Cu<sub>2</sub>O. They synthesized the round shaped gold nanocrystals with opposite corner distance of 41 and 57 nm and the nanocube, octahedral Au-Cu<sub>2</sub>O using hydrothermal method<sup>37</sup>. But the nanobars were synthesized by the seed-mediated growth method. Au nanorods were added during the synthesis of Cu<sub>2</sub>O<sup>37</sup>. The absorption band of nanocubes and octahedral Au-Cu<sub>2</sub>O having a surface plasmon resonance (SPR) in the near-infrared (NIR) region from Au core with octahedral shape having SPR band around 808 nm were used for light excited heat production. The cube shape Au-Cu<sub>2</sub>O solution upon irradiation could reach 65° C after 5min. The surface plasmon resonance band of their Au domains matches that of the illuminating light wavelength. In the case of nanobars, gold nanorods, were used that has {100} facet bounded in Au-Cu<sub>2</sub>O hybrid with promising tunable longitudinal Au SPR absorption band in the broad NIR range from approximately 1050 to 1400 nm, hence displaying a much better photothermal properties<sup>38</sup>.



**Scheme 1**, Image of Cu<sub>2</sub>O Shell with Au Core<sup>38</sup>

Yang et al., reported that the absorption band of Au surface plasmon resonance in the Au-Cu<sub>2</sub>O heteronanostructures depend on the surface facets of single crystalline Cu<sub>2</sub>O shells. The light scattering effect of the Cu<sub>2</sub>O shell was minimized due to its small crystallite size which enable the easy identification of the surface plasmon resonance (SPR) absorption band of the Au cores and the thickness of the Cu<sub>2</sub>O shell. There was no effect of shell thickness on the SPR absorption band of Au, beyond the lower shell limit required, but it depends strongly on the exposed particle surfaces<sup>39</sup>.



**Scheme 2**, Au@Cu<sub>2</sub>O photocatalytic effect<sup>39</sup>

The research work by Pan et al., dwells on the surface functionalization of nanocomposites by functional groups such as amine, thiol and carboxylates, which provides a linkage between the noble metal and the semiconductors hybrid. Specifically, a poly( $\sigma$ -anisidine)-

capped Cu<sub>2</sub>O nanowires (NWs) were used to provide a very strong hydrophobic host-guest interaction with oleylamine-capped Au NPs to form metal-semiconductor which enabled the separation of nucleation of free nanocrystal and the control of the size of the Au NWs. Also the photodegradation of methylene blue was tested in aqueous solution for these hybrid materials. Pristine Cu<sub>2</sub>O NW exhibited very low photocatalytic activity as compared to Au-Cu<sub>2</sub>O nanocomposites. The time-resolved photoluminescence spectroscopy was used to probe the surface electron process at the heterostructure interface<sup>37</sup>.

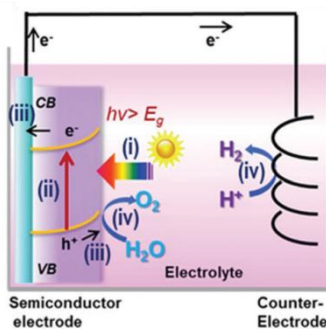
Cuprous oxide (Cu<sub>2</sub>O) is a p-type semiconductor. The vacancies in Cu enable it to accept electron, bases on which it was hypothesized that Cu<sub>2</sub>O is a p-type semiconductor,<sup>38</sup> with theoretical and experimental facts support the hypothesis has gain widely acceptance<sup>39,40</sup>. However, controversy still lace the exact nature of the vacancies in copper. Papadimitriou earlier reported, by the use of dep-level transient spectroscopy (DLTS) that the hole traps were associated to CuO reefs<sup>40</sup>. Paul, recently, use DLTS in the identification of two trap states in Cu<sub>2</sub>O, which was attributed to single and double Cu vacancies<sup>41</sup>. Also, it was observed and reported that the electric conductivity was due to single Cu Vacancies i.e. two 3-fold coordinated oxygen with one Cu missing or split Cu vacancies, this implies neighboring Cu atom moves toward Cu vacancy and coordinates four oxygen's, this assertion is credited to scientist, although, the disagree on which of the possibilities is more stable thermodynamically<sup>42,43</sup>. The formation energies of the oxygen interstitials, other intrinsic acceptors in either octagonal or tetragonal coordination are much higher than for vacancies.

Wan-Chen, reported the synthesis of Cu<sub>2</sub>O in cubic, octahedral, and rhombic structure, working in room condition, in aqueous medium by using surfactant sodium dodecyl sulfate

(SDS), Copper (2) oxide chloride ( $\text{CuCl}_2$ ), sodium hydroxide ( $\text{NaOH}$ ), reductant  $\text{NH}_2\text{OH}\cdot\text{HCl}$  and each morphology was tested on methyl orange to grade there photodegradation and state the inability of facet with  $\{100\}$  face to degrade methyl orange<sup>44</sup>. The *in-situ* growth of noble metal nanoparticles onto semiconductor, in which  $\text{Cu}_2\text{O}$  was synthesis using wet-chemical reduction and the subsequent introduction of the noble metal to a targeted facet of the semiconductor was reported.  $\text{Cu}_2\text{O}$  nanotubes were prepared by adding  $\text{CuCl}_2$  and  $\text{NaOH}$ , into distilled water under magnetic stirring and- ascorbic acid was added as reducing agent, the contents were further stirred for 15min to harvest  $\text{Cu}_2\text{O}$  nanocube. The product was washed then noble metal solution was added to achieve the desired hybrid product.<sup>45</sup>

Fujishima and Honda, for the first time, discovered  $\text{TiO}_2$  as PEC active catalyst with  $\sim 0.1\%$  quantum efficiency<sup>46</sup>. Since then there is a steady progress in the field with respect to both materials synthesis and engineering of the PEC setups, thereby reaching the efficiencies of  $12.7\%$  using a p-GaInP<sub>2</sub>/GaAs as photoanode material or  $14\%$  using a Z-scheme tandem cell having Rh-engineered AlInPO<sub>x</sub> photocathode and  $\text{RuO}_2$  as photoanode<sup>47,48</sup>. It is worth mentioning, although the choice of materials plays a role for the successful harvesting of solar energy but it is the surface engineering of materials which defines its practical applicability<sup>49</sup>. For example, to harvest the maximum range of solar spectrum, materials having bandgap between  $1.6$  and  $2.4$  eV could be meritorious but they are chemically unstable on photo-excitation under aqueous environments such as photoelectrochemical (PEC) water splitting<sup>50</sup>. Therefore, we need to tailor the surfaces to exploit the full available potential.

There are four main features which defines the overall success of PEC water splitting reaction; **(i)** band gap energy and the conduction and valence band edge positions, **(ii)** transportation of the exciton to the surface, **(iii)** separation of charge carriers, and **(iv)** surface reaction leading to stable product as shown in Scheme 3<sup>51</sup>. The three among these four decisive factors not only depend on the chemical composition but also the size, morphology, crystallinity and surface chemistry of photoelectrode materials.



**Scheme 3:** Schematic illustration of the photoelectrochemical cell operation using n-type semiconductor; the water splitting reaction steps (i–iv) reproduced from the Kment et al<sup>51</sup>.

Among semiconductors,  $\text{Cu}_2\text{O}$  with small band gap  $\sim 2.1$  eV and suitable conduction band edge position, naturally abundant, cost efficient, non-toxic fulfils all the basic criteria required for photocatalysis and water splitting<sup>52</sup>. Although intrinsically,  $\text{Cu}_2\text{O}$  is p-type semiconductor but it can be synthesized as n-type by varying the reaction conditions and methodology<sup>57</sup>. Owing to its technological importance, the progress for the synthesis of  $\text{Cu}_2\text{O}$  nanostructures is documented, especially facet dependent catalytic applications of  $\text{Cu}_2\text{O}$  based particles<sup>53</sup>. However, most of these synthetic methods resulted in microsize particles.  $\text{Cu}_2\text{O}$  in combination with metal and metal oxide as hetero-particles have also been tested and showed better results but still these reports were significantly below the

theoretically expected photocurrent density ( $14.5 \text{ mA cm}^{-2}$ )<sup>54-56</sup>. There are two main drawbacks for using  $\text{Cu}_2\text{O}$  in practical applications: **(1)** short carrier diffusion length (20-100 nm) upon light absorption (related to particles size) and **(2)** its self-photocorrosion upon contact with water (surface chemistry).

### 2.1.1 Statement of Problem

Environmental concern associated with energy generation from fossil fuel and its limited supply, warrant a new frontier, hoped at replacing the current source of energy to a safe, clean and sustainable source of energy. Materials that can find usefulness in this area of study is currently being searched and developed across the globe. Copper (1) Oxide captured our interest for its uniqueness as a visible light spectrum harvester, a semiconductor, with band gap of about 2.1eV suitable to serve the intended purpose of harvesting the maximum portion of sunlight spectrum.

We will also introduce plasmonic metal to further boost visible spectrum harvesting ability of the semiconductor ( $\text{Cu}_2\text{O}$ ) nanoparticle, and the morphology of interest is cube and octahedral that will be tested against organic dye like methyl blue (ME) contaminated water. Bearing in mind, the key role of absorption step in the pollutant removal process, the unique morphology of the synthesis  $\text{Cu}_2\text{O}$  with active facets exhibit excellent adsorption performance.

### 2.1.2 Project Objectives

The main objective of the project is to develop nanostructured  $\text{Cu}_2\text{O}$ ,  $\text{Au}/\text{Cu}_2\text{O}$  hybrid nanoparticles for visible light catalyzed applications.

In contribution, we will concentrate on the following objectives;

1. Optimization of the synthesis of  $\text{Cu}_2\text{O}$  nanoparticles and  $\text{Au}/\text{Cu}_2\text{O}$ , hybrid nanoparticles with various sizes and morphologies of both Au and  $\text{Cu}_2\text{O}$  components.
2. Characterization of the as-prepared hybrid nanoparticles using various advanced spectroscopic (UV-Visible, photoluminescence), scanning electron microscopy (SEM), and X-ray based techniques.
3. Engineering the surface of  $\text{Cu}_2\text{O}$  with focus to maximize harvesting the solar spectrum and to minimize photo-corrosion on contact with water through synthesis hybridization of Au on the surface of pristine  $\text{Cu}_2\text{O}$  nanoparticles.
4. Photocatalyzed degradation of organic pollutant using these hybrid nanoparticles.
5. Compilation of the data for future exploration of industrial application of the synthesized nanocomposite materials.

## **CHAPTER 3**

### **RESEARCH METHODOLOGY**

Hydrated copper (II) chloride ( $\text{CuCl}_2 \cdot 2\text{H}_2\text{O}$ , 97%) and hydroxylamine hydrochloride ( $\text{NH}_2\text{OH} \cdot \text{HCl}$ ; 99%) were purchased from Aldrich. Sodium dodecyl sulfate (SDS) were acquired from Mallinckrodt, Sodium hydroxide (NaOH) was gotten from Fluke, Ethylene glycol ( $\text{HOCH}_2\text{CH}_2\text{OH}$ ) was purchased from Fisher, Copper Acetate ( $(\text{Cu}(\text{CH}_3\text{COO})_2)$ ), Glucose ( $\text{C}_6\text{H}_{12}\text{O}_6$ ), Ethanol ( $\text{CH}_3\text{CH}_2\text{OH}$ ) were purchased from Aldrich. All chemical was used as purchase without further purification. Deionized water gotten from research institution of king Fahd university of petroleum and minerals.

#### **3.1 Nanomaterial Synthesis**

The proposed project includes the synthesis of hybrid nanoparticles containing copper, oxygen and Au. The metal oxide ( $\text{Cu}_2\text{O}$ ), optimization of size, morphology and crystal structure and its hybridization with Au to form hybrid materials. This would be realized by controlling the nucleation and growth process of these components employing non-aqueous as well as aqueous medium. These materials are used as photocatalyst for organic dye degradation. The research methodology was divided in three different steps.

##### **3.1.1 Synthesis of $\text{Cu}_2\text{O}$ , Au@ $\text{Cu}_2\text{O}$ Based Multi-Component Nanomaterials**

##### **3.1.2 Non-Aqueous Synthesis**

The synthesis for the formation of nanoparticles proceeds through bottom-up non-aqueous high temperature solution method. Non-aqueous high temperature solution

syntheses have been developed to control the size, morphology, faceting, crystallinity and surface functionalities of such nanomaterials<sup>23,57</sup>. The non-aqueous synthesis is especially helpful for the synthesis of nanoparticles because the reaction kinetics can be easily controlled by taking snapshot of the reaction by monitoring the chemical events through changes in physical appearance, spectroscopically or microscopically. This helps to control the nucleation and growth process which are the key parameters to easily add/incorporate multiple domains in a single nanoparticle so called multicomponent or heterostructure nanoparticle.

In a rinse and oven dried breaker, 4ml ethylene glycol and 0.024g (0.37mmol) of copper acetate was added sequentially, stirred, then 4ml ethylene glycol, again stirred before sonication, and 8ml of ethylene glycol, follow by the addition of 0.024g (0.37mmol) of glucose to facilitate reduction of copper (II) to copper (I). Sonication continued for 20min, more 24mg of glucose was added, the reaction temperature was set at 40<sup>0</sup>C, expected color change not observed then 0.5mg glucose was introduce and finally the nanoparticles were washed with ethanol.

In an attempt to achieve the expected nanoparticle, the stated procedure was adjusted, into a round bottom flask; ethylene glycol (8ml), followed by the addition of copper acetate immediately. The mixture was placed in the sonicating water bath set at 50<sup>0</sup>C and sweeping vibration mode, when a clear solution is formed, 148mg of glucose was added and the flask was covered with a septum rubber, a balloon filled with nitrogen gas was connected through the septum into the flask using a needle.

Copper(II)chloride, benzoyl alcohol and Sodium hydroxide was used in this synthesis procedure; 20mg  $\text{CuCl}_2$ , was poured into an 8ml benzoyl alcohol ( $\text{C}_6\text{H}_5\text{CH}_2\text{OH}$ ) in a flask, under stirring till the temperature reaches  $60^\circ\text{C}$ , at about 45min of reaction time NaOH in ethanol was added dropwise. Figure 5, is the UV-Vis-spectra of copper oxide synthesis using non aqueous medium, where it is observed that there was no absorption related to  $\text{Cu}_2\text{O}$  phase, that normally lies in the visible region around 450nm – 550nm.

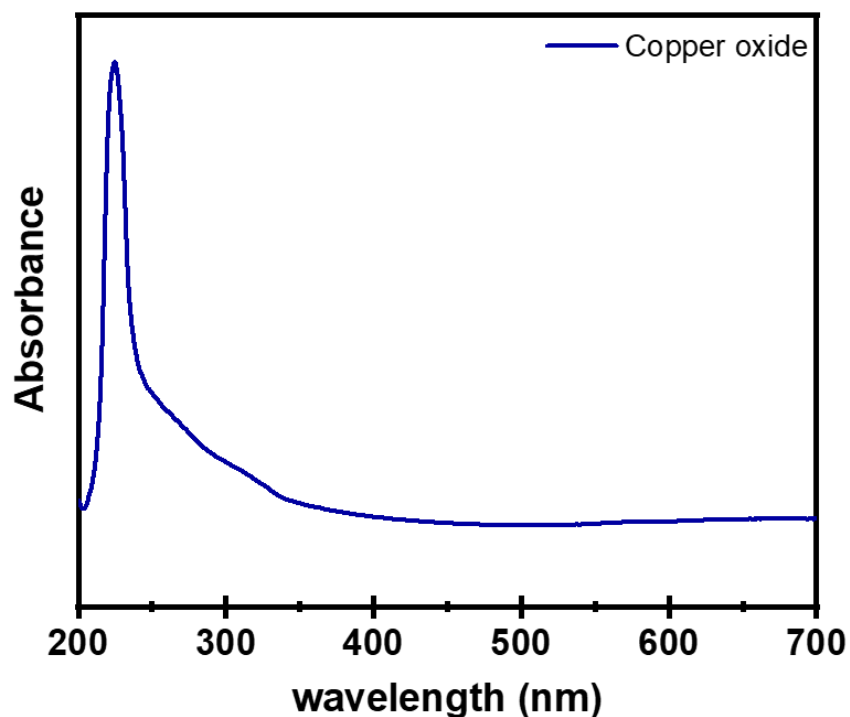
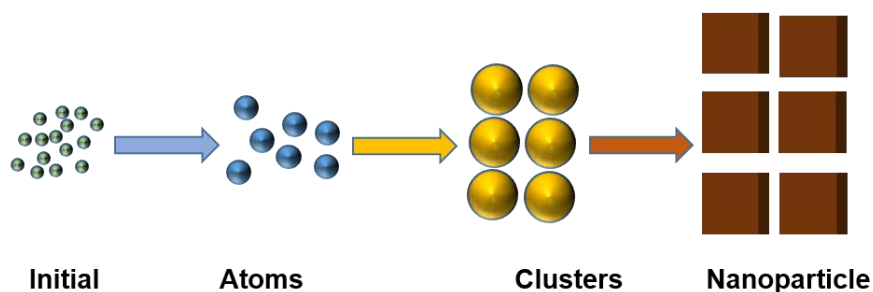


**Figure 5**, UV-Vis Spectra of Non-Aqueous Synthesized cube shaped  $\text{Cu}_2\text{O}$

### 3.1.3 Aqueous Synthesis

The synthesis of hybrid nanoparticles was accomplished by employing bottom-up aqueous room temperature solution synthesis method. Sonication assisted, with temperature around 30-35<sup>0</sup>C, syntheses have been developed to control the size, morphology, faceting, crystallinity and surface functionalities of Au and Cu<sub>2</sub>O hybrid materials nanomaterials. The aqueous synthesis is especially helpful for the synthesis of multicomponent nanoparticles because the reaction kinetics can be easily controlled by taking snapshot of the reaction by monitoring the chemical events through changes in physical appearance, spectroscopically or microscopically. This helps to control the nucleation and growth process which are the key parameters to easily add/incorporate multiple domains in a single nanoparticle so called multicomponent or heterostructure nanoparticle. Scheme 4, shows the bottom-up approach of nanoparticle synthesis.



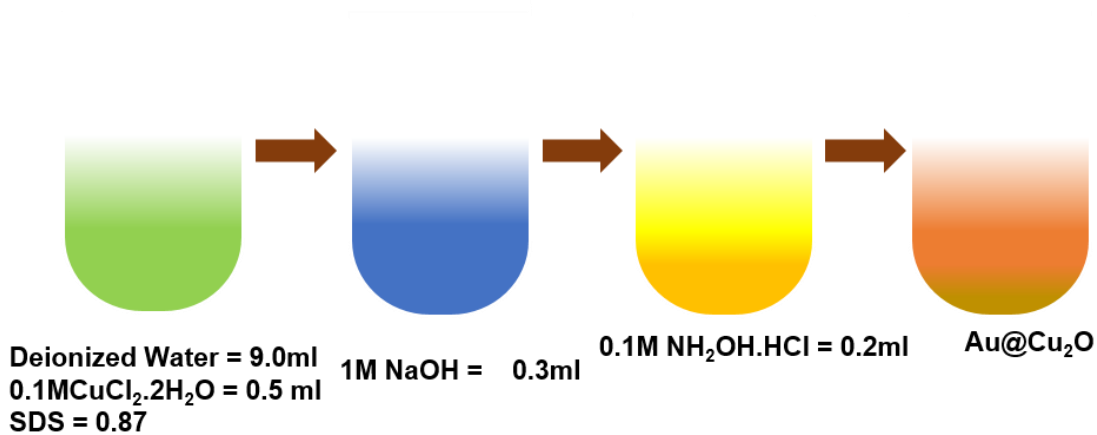
**Scheme 4**, Bottom-up synthesis of nanoparticle

### 3.1.4 One Step Synthesis

In one step synthesis of Au@Cu<sub>2</sub>O hybrid nanoparticles, metal nanoparticles would be synthesized *in situ* using benzyl alcohol as a solvent and oleyl amine as reducing agent using chloroauric acid or copper acetate or copper acetylacetonate as precursor compounds<sup>15</sup>. The growth of Cu<sub>2</sub>O domain would be realized by heating up method and

growth of Au or Cu domains onto preformed metal oxide nanoparticles acting as seed particles<sup>14,15,23,32</sup>. The number of domains of metal components attached to single particle will be controlled by changing the solvent polarity to localize the surface plasmons of metal component onto the surface of Cu<sub>2</sub>O NPs as demonstrated by the author and many other researchers for the synthesis of other metal@metal oxides based multicomponent nanoparticles<sup>15, 32</sup>. The one-step synthesis is shown in scheme 2 below.

A round bottom flask was used as the reaction apparatus, into which 9.0ml deionized water was added, 0.5ml of 0.1M CuCl<sub>2</sub>.2H<sub>2</sub>O introduced, this was followed by the addition of sodium dodecyl sulfate (SDS) and placed into a sonicates water bath set at 35<sup>0</sup>C temperature and vibration time of 20min, as the SDS fully dissolve, as shown in Scheme 5, a light greenish color was noticed and 0.3ml of 1M NaOH was added and the mixture color changes to blue, when 0.2ml of 0.1M NH<sub>2</sub>OH.HCl was added into the mixture, the color immediately changes to yellow. This signifies the formation and subsequent growth of nanoparticle which is the copper (I) oxide (Cu<sub>2</sub>O). finally, 1ml of 0.002mM HAuCl<sub>4</sub> was added to form gold deposited nanomaterial hybrid, after 1hour growth time, Au-Cu<sub>2</sub>O was collected through centrifuge by washing with deionized water, and ethanol.



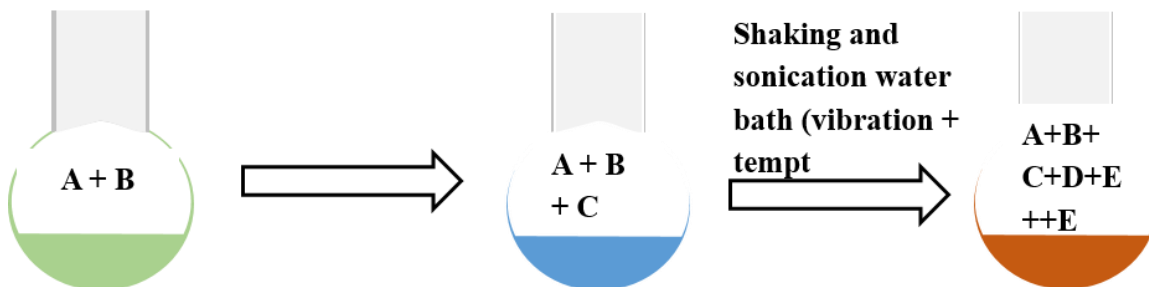
**Scheme 5**, Schematic of In-situ synthesis cube and octahedron shaped Cu<sub>2</sub>O

### 3.1.5 Two Step Synthesis

The two step synthesis involves the synthesis of metal oxide nanoparticles separately in the first step followed by growth of metal components. The *in situ* synthesis of metal domains in multicomponent nanoparticles gives less control to play the size and morphology of these metal nanoparticles. To elucidate the influence of the size and morphology of plasmonic domains on the overall performance of photoelectrode in the present project, in the first step the Cu<sub>2</sub>O with various size and shapes shall be synthesized separately. These nanoparticles shall be used as seed particles to grow metal domains in the second step. Moreover, the sizes of different components and number of metal domains grown onto Cu<sub>2</sub>O domain will be varied by proper choice of precursors compounds to surfactant ratios, nature of solvent and reaction kinetics as demonstrated by the author for other metal@metal oxides based multicomponent nanoparticles<sup>15,21</sup>.

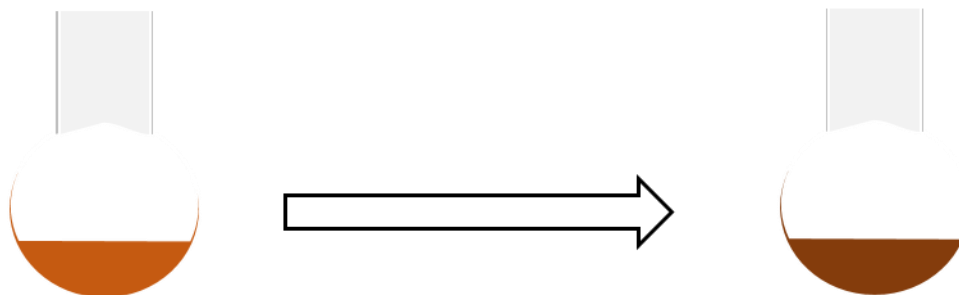
The synthesis of cube shaped Cu<sub>2</sub>O nanoparticles was carried out in dried round bottom flask using 2ml of the freshly prepared 0.1M solution of CuCl<sub>2</sub>.2H<sub>2</sub>O, 11ml deionized water and 0.48g sodium dodecyl sulfate (SDS) was added slowly under shaking on span of few minutes, before it was placed on a sonication water bath, set at 35<sup>0</sup>C and vibration time for 10min. Immediately the vibration stops, 1ml of 1.0M NaOH was added randomly, the vibration of the sonication water bath was turn-on again, then 1.6ml of 0.1M NH<sub>2</sub>OH.HCl was added randomly and the vibration was allowed to stop. The nanoparticles are allowed to grow under aging process for 1hour. The nanoparticles were collected by first washing three times with deionized water to remove the unreacted reactant follow by washing twice with ethanol and the nanoparticle was stored in a sample vial.

In Scheme 6, synthesis route of copper (I) oxide. A = DI Water, B =  $\text{CuCl}_2 \cdot 2\text{H}_2\text{O}$ , C = SDS, D = NaOH, E =  $\text{NH}_2\text{OH} \cdot \text{HCl}$  and  $\text{A+B+C+D+E} = \text{Cu}_2\text{O}$ .



### Scheme 6, Cube morphology $\text{Cu}_2\text{O}$ nanoparticle synthesis

The product from scheme 6, was washed with deionized water several times to remove unreacted substance, this was transferred into a round bottom flask using 10ml deionized water, and placed on a sonication water bath set at  $35^\circ\text{C}$  temperature with vibration time of 10min, as the vibration stops, 0.3ml of 0.001M  $\text{HAuCl}_4$  was added as shown in scheme 7 the color change to brown.



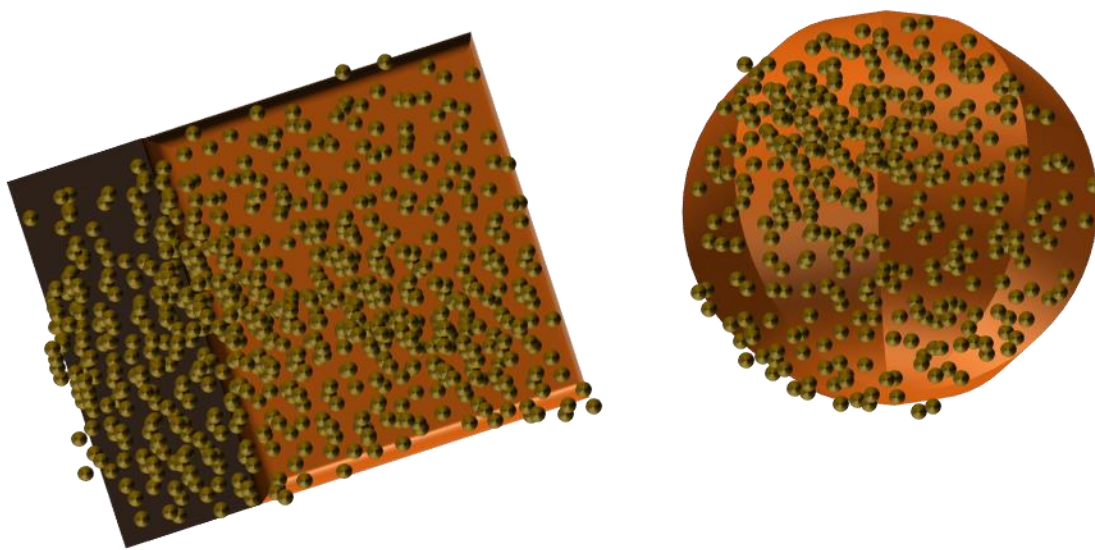
### Scheme 7, Cube Shaped $\text{Cu}_2\text{O}$ nanoparticle, decorated with Au Nanoparticle.

#### 3.1.6 Synthesis of $\text{Au}@\text{Cu}_2\text{O}$ Hybrid Nanoparticles

The second methodology to stabilize the  $\text{Cu}_2\text{O}$  surface from photo-corrosion as well as enhance visible light harvesting efficiency is being based on growth of the few Au

nanoparticles on the surface of  $\text{Cu}_2\text{O}$  domain. This was achieved through injection of Au or Ag precursor at suitable time while the  $\text{Cu}_2\text{O}$  domain has developed.

A schematic presentation for the synthesis of proposed materials is shown in Scheme 8.



**Scheme 8,** Schematic representation of the synthesis of heterodimer and multimers  $\text{Au}@\text{Cu}_2\text{O}$  hybrid nanoparticles

In order to synthesize cube and octahedral morphology of  $\text{Cu}_2\text{O}$  with decorated gold nanoparticles as shown in scheme 5, 50ml round bottom flask was charged with 11ml deionized water, 0.6ml of  $\text{CuCl}_2 \cdot 2\text{H}_2\text{O}$  (0.1M) and 0.087g sodium dodecyl sulfate (SDS). The mixture is kept on shaking before set on sonication (Temperature  $35^\circ\text{C}$ , Vibration 25min), as the SDS dissolved, 1.5ml of 1M NaOH was added for cube while to obtain octahedral shape  $\text{Cu}_2\text{O}$ , 1.2ml was added, follow by 3ml of 0.1M  $\text{NH}_2\text{OH} \cdot \text{HCl}$  and sonication continue for few minute. The color change from blue to deep yellow and nanoparticle is allowed to grow by again for 1 hour and then washed with deionized water three times. The resulting nanoparticles were transferred back into the round bottom flask

with 10ml deionized water sonicate for few minute before 0.3ml HAuCl<sub>4</sub> (0.001m) was added into it and the hybrid nanomaterial is allowed to grow.

### **3.1.7 Characterization of Multi-Component Nanoparticles**

To confirm the size, shape, composition, phase and optical properties of the as synthesized materials will be characterized using SEM, TEM, XRD and UV-visible spectroscopy.

#### **Photocatalytic applications**

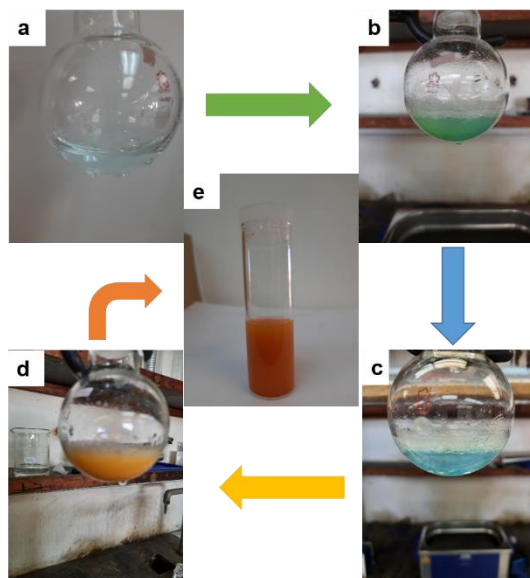
The hybrid nanoparticles are used for visible light assisted photo-catalysis for the degradation of organic pollutants in water as well for the water splitting reaction. For the photoelectrochemical (PEC) splitting of water, the photoelectrodes shall be fabricated on FTO substrates using drop casting (due to the colloidal nature of proposed materials). The photoelectrode surfaces and thickness will be characterized using scanning electron microscopy (SEM). Their photo-electrochemical efficiency shall be tested using Pyrex container 3-electrode cell with a 0.5 M Na<sub>2</sub>SO<sub>4</sub> electrolyte (pH 7.0 ± 0.1) connected to argon gas cylinder. A Pt wire as auxiliary electrode), FTO coated with different M-Cu<sub>2</sub>O hybrid composites as working electrode, and a saturated calomel electrode (SCE) as reference electrode.

# CHAPTER 4

## RESULTS AND DISCUSSIONS

### 4.1 Spectroscopy Characterization

The structure and composition of the nanoparticles were probed to have a deep insight on the fundamental properties of the synthesized nanomaterials with different morphologies towards the photocatalytic degradation of methylene blue and photoelectrocatalytic splitting of water. Spectroscopic characterization was performed to get full grasp of usefulness of  $\text{Cu}_2\text{O}$  and  $\text{Au@Cu}_2\text{O}$  in different applications and the importance of the morphologies and their hybridization of the semiconductor nanoparticle with noble metal in boosting the stability and efficiency of the nanomaterials. The kinetics of the as synthesis  $\text{Cu}_2\text{O}$  and the hybrid  $\text{Au@Cu}_2\text{O}$  are monitored to have a quality insight on the reaction transition from the initial to the final stage. This is observed through color changes that occurs as each reactant were introduced into the synthesis pot. Starting from the colorless deionized water (Scheme 9a), to a light green color on addition of surfactant (SDS) (Scheme 9b), the color becomes blue as a base (NaOH) is introduced indicating the production of more OH ions (Scheme 9c), and the addition of the reducing agent ( $\text{NH}_2\text{OH.HCl}$ ) changes the color to yellow (Scheme 9d), finally as the nanoparticle grow the color of the reaction becomes orange (Scheme 9e).



**Scheme 9**, Shows the synthesis steps with the corresponding color changes, from colorless through light green, blue, yellow and finally orange color.

## 4.2 Scanning Electron Spectroscopy (SEM) Image

The morphology of the synthesized nanoparticles both pristine and as well as decorated with Au nanomaterial were obtained using high-end-field emission scanning electron microscope (FESEM, Tescan-Lyra-3) in the department of chemistry of King Fahd University of Petroleum and Minerals. The samples were well prepared to ensure they are stabilized and possess electrical conductivity their insertion the SEM chamber to record SE micrographs. Scanning electron microscope (SEM) is a technique that uses a focused radiation of high energy electrons to produce several coherent signal at the surface of the well prepared dried sample of the nanomaterial. The signals that emerge from the electron-nanomaterial interactions exposes the information about the nanomaterial orientation, crystallinity structure, chemical composition and it topography. The accelerated electrons generated in SEM are energetically strong enough to dissipate, several signal through the electron-nanoparticle interaction when the incident electrons are

decelerated. The signals used by a scanning electron microscope to generate result from beam atoms interaction at various depths within the nanomaterial can be of several types, such as secondary electrons (SE) which have a low energy on the order of 50 eV, which limits their mean free path in nanoparticle, back-scattered electrons (BSE) and diffracted backscattered electrons (EBSE) are beam electrons that are reflected from the nanoparticle elastic scattering, and are valuable in illustrating contrasts in composition of multiphase sample. Figure 6-13, shows the SEM image of all the synthesized morphologies for both Cu<sub>2</sub>O as well as Au@Cu<sub>2</sub>O hybrid versions. SEM image (Figure 6) represent cube Cu<sub>2</sub>O that was synthesized without the addition of sodium dodecyl sulfate (SDS). In the absence of surfactant SDS, the expected morphology was not achieved. It resulted in irregular shape with broad size distribution. Figure 7-9 shows the as synthesized Cu<sub>2</sub>O upon addition of surfactant sodium dodecyl sulfate in the synthesis procedure at varying amount, (Figure 10) correspond to the cube shape image of Au decorated Cu<sub>2</sub>O, (Figure 11) SEM image of octahedral shape Cu<sub>2</sub>O, and Figure 12 show the image of octahedral Cu<sub>2</sub>O, (Figure 13) the SEM for the Au decorated Cu<sub>2</sub>O with octahedral crystallinity structure.

The SEM image show (Figure 6) that a dark cubic Cu<sub>2</sub>O of 10 μm sized nanoparticle with lot of dirty like wool material covering which can be undoubtedly attributed to the in ability of the reactant to be exhaustively utilized in the cause of the reaction, as the reacting medium, in this case deionized water could not facilitate the complete mix ability of the precursor salt, the base and the reducing agent. This was the consequence of not using surfactant SDS, which would have allowed for the proper reactant interactions.

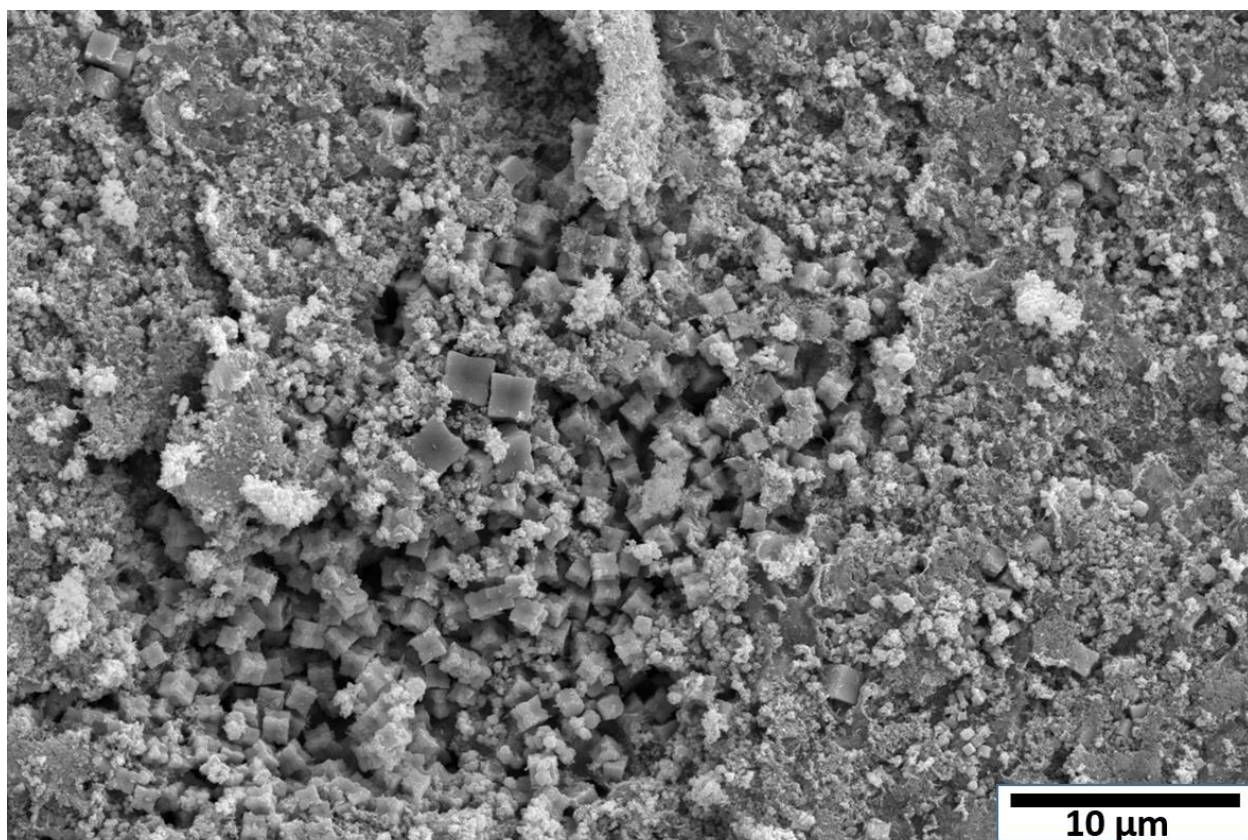


**Figure 6**, SEM image of the  $\text{Cu}_2\text{O}$ , synthesized without sodium dodecyl sulfate (SDS), a surfactant.

The established image (Figure 6) that resulted when surfactant (SDS) was not used in the synthesis of  $\text{Cu}_2\text{O}$  necessitated the need to add a controlled amount of SDS in the subsequent reaction. Figure 7, show an improved SEM image  $\text{Cu}_2\text{O}$  with more uniform size, preferably clear than the previous synthesized nanoparticle without using SDS. The nanoparticle is about  $10\ \mu\text{m}$ , and the tread like material on the  $\text{Cu}_2\text{O}$  cube are from the unreacted reactant courtesy of the control amount of the added surfactant.

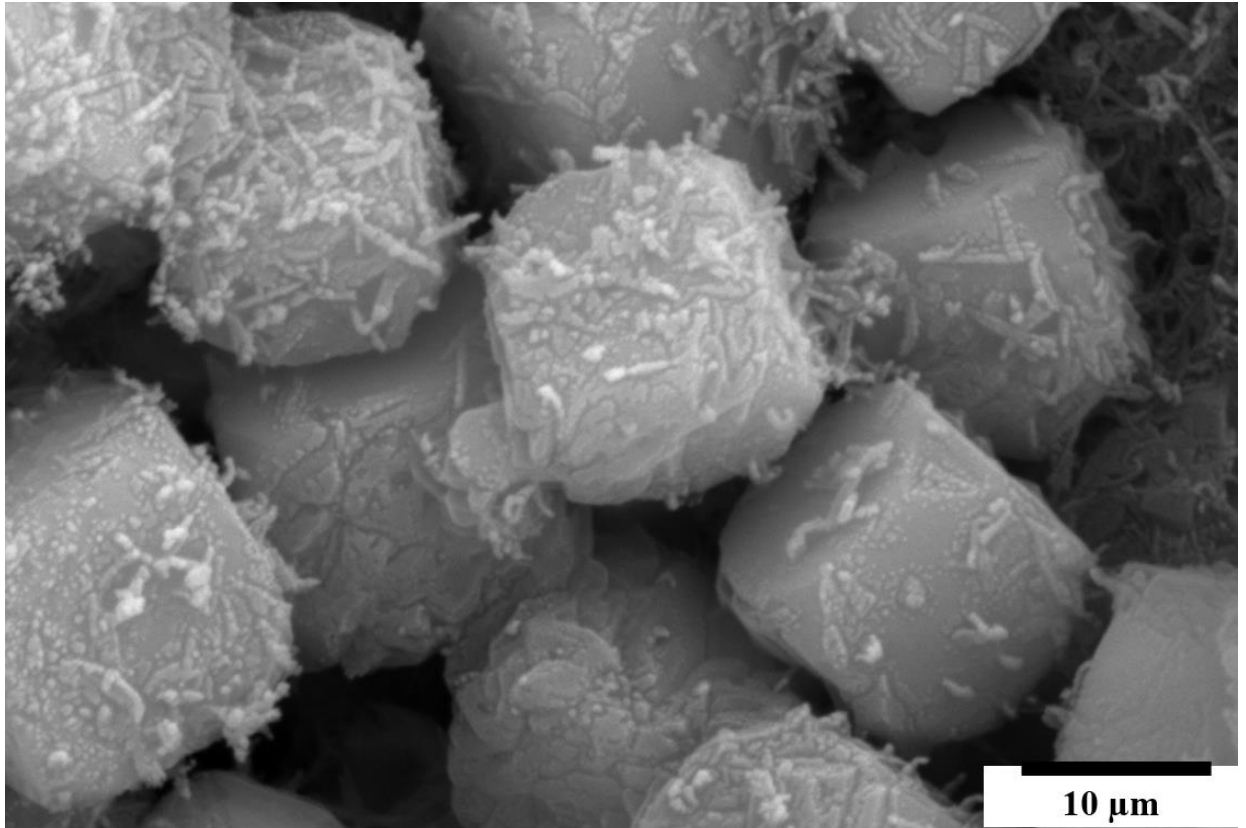


**Figure 7,** Bears the SEM image of Cube Cu<sub>2</sub>O synthesized with addition of 0.087mg of SDS.

Upon increasing the amount of SDS as surfactant, a monomorphic cube shape Cu<sub>2</sub>O nanoparticle as shown in Figure 8 are obtained. The average size of the nanoparticles was about 3 μm. The SEM image reflect an improvement in control on size as well as the cleanness of the nanoparticle facet with the right amount of surfactant used during synthesis and the proper dissolution of the surfactant before the addition of base for pH adjustment.

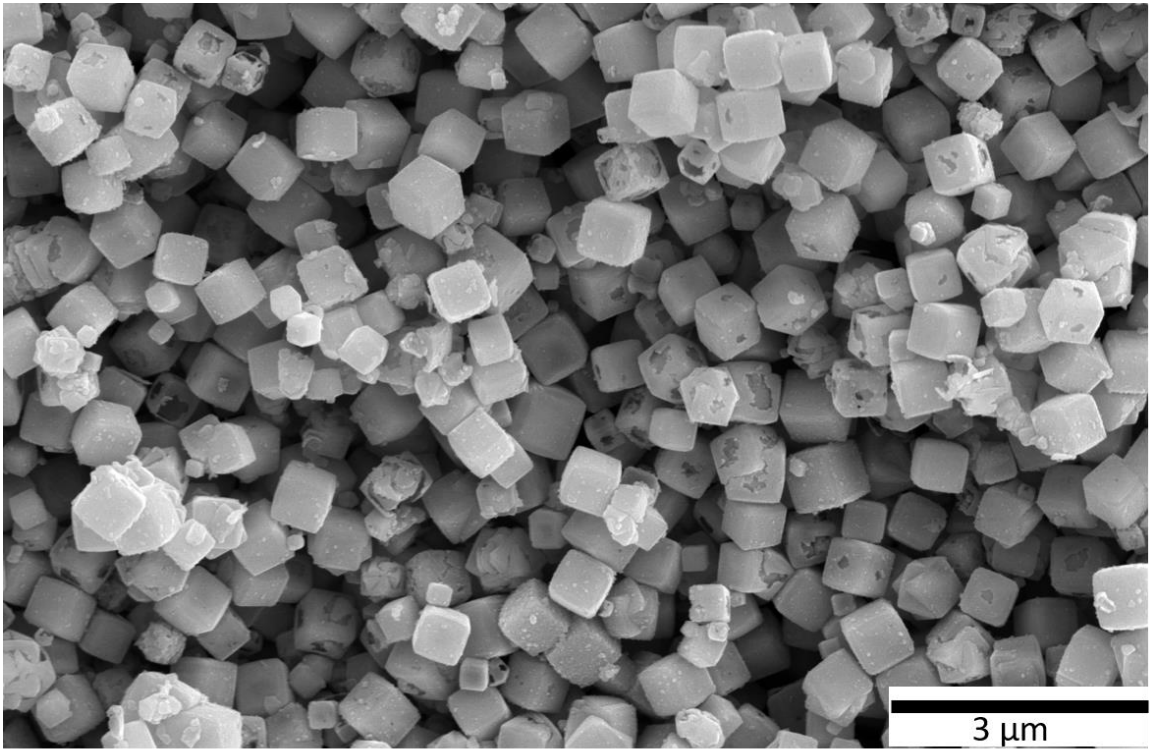


**Figure 8**, SEM image of Cube  $\text{Cu}_2\text{O}$  with all reaction condition maintained

As more growth time for the as prepared nanoparticle, this further show (Figure 9) the clear cubic morphology of the synthesized  $\text{Cu}_2\text{O}$ .

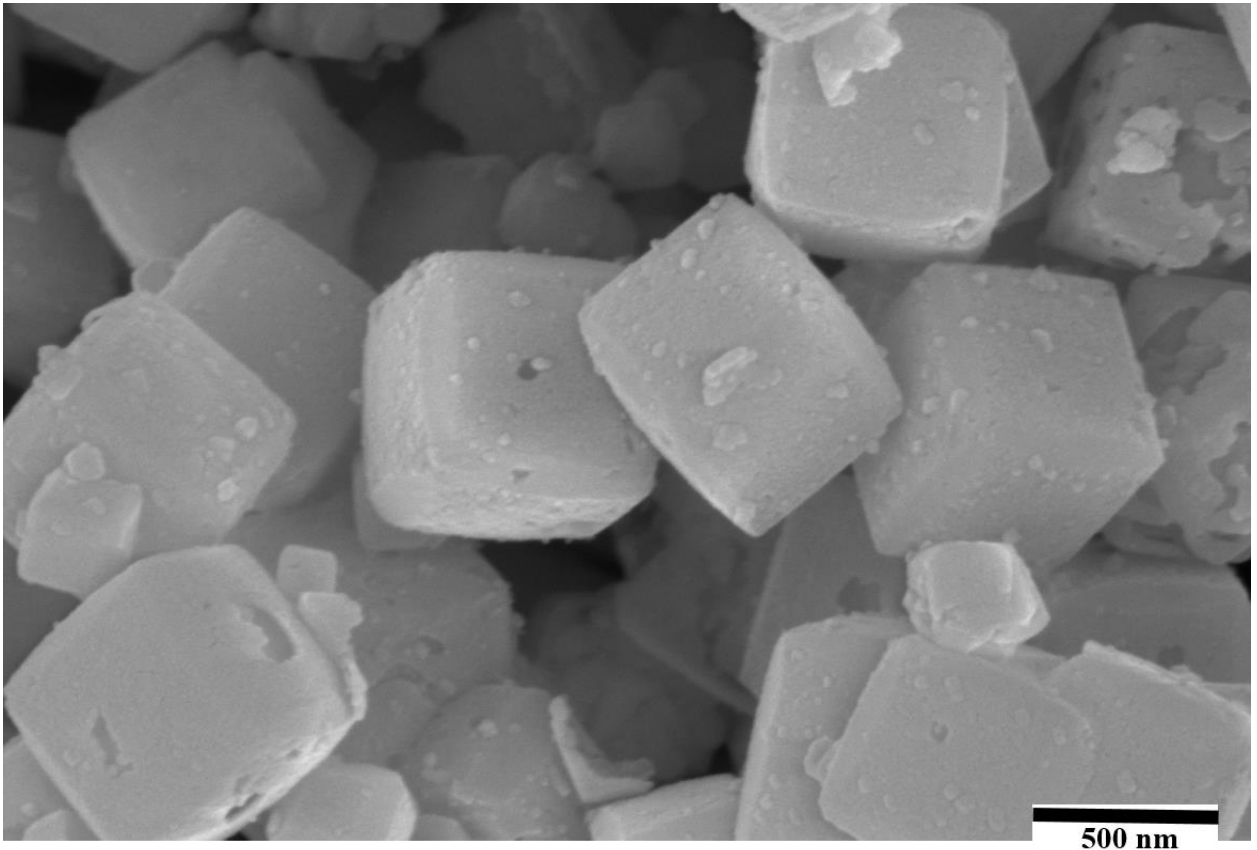


**Figure 9**, SEM image of cube Cu<sub>2</sub>O nanoparticle with synthesis longer growth time.

The scanning electron microscopy (SEM) image (Figure 10) show the achieved carefully deposition of gold (Au) on a cubic Cu<sub>2</sub>O, the facet of Au growth on the copper oxide tallies with the result from XRD, that shows the selective deposition of Au on a certain Cu<sub>2</sub>O lattice plane, the plane is (111), (200), (220), and (311). EDS mapping also show how well dispersed deposited the is the Au nanoparticle on the cubic plane of the semiconductor Cu<sub>2</sub>O, from which it was confirmed that the percentage of Au nanoparticle was 0.7% that bided to the selected lattice plane of the cube Cu<sub>2</sub>O nanoparticle.

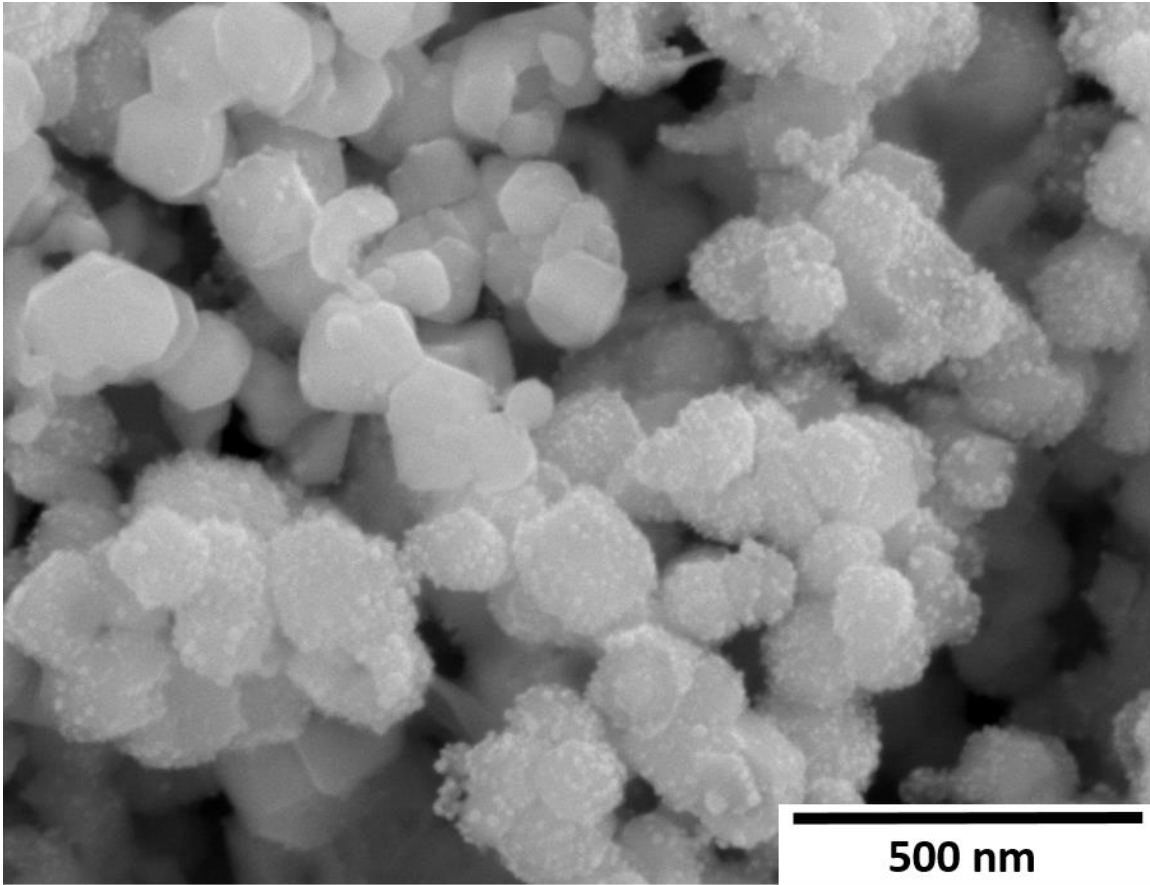


**Figure 10**, SEM image of cube  $\text{Cu}_2\text{O}$  semiconductor, that is decorated with Au nanoparticle (Au@ $\text{Cu}_2\text{O}$  hybrid nanomaterials)

The SEM image of pristine (Figure 11) octahedral  $\text{Cu}_2\text{O}$  is shown. A nanoparticle of  $1\ \mu\text{m}$  size octahedral semiconductor consisting of copper and oxygen with an octahedral shape was synthesis using reaction procedure similar to the cubic semiconductor reaction condition of  $35^\circ\text{C}$  temperature with sonication vibration of 20 min and reactant addition sequence, at an appropriate nanoparticle growth time of an hour.

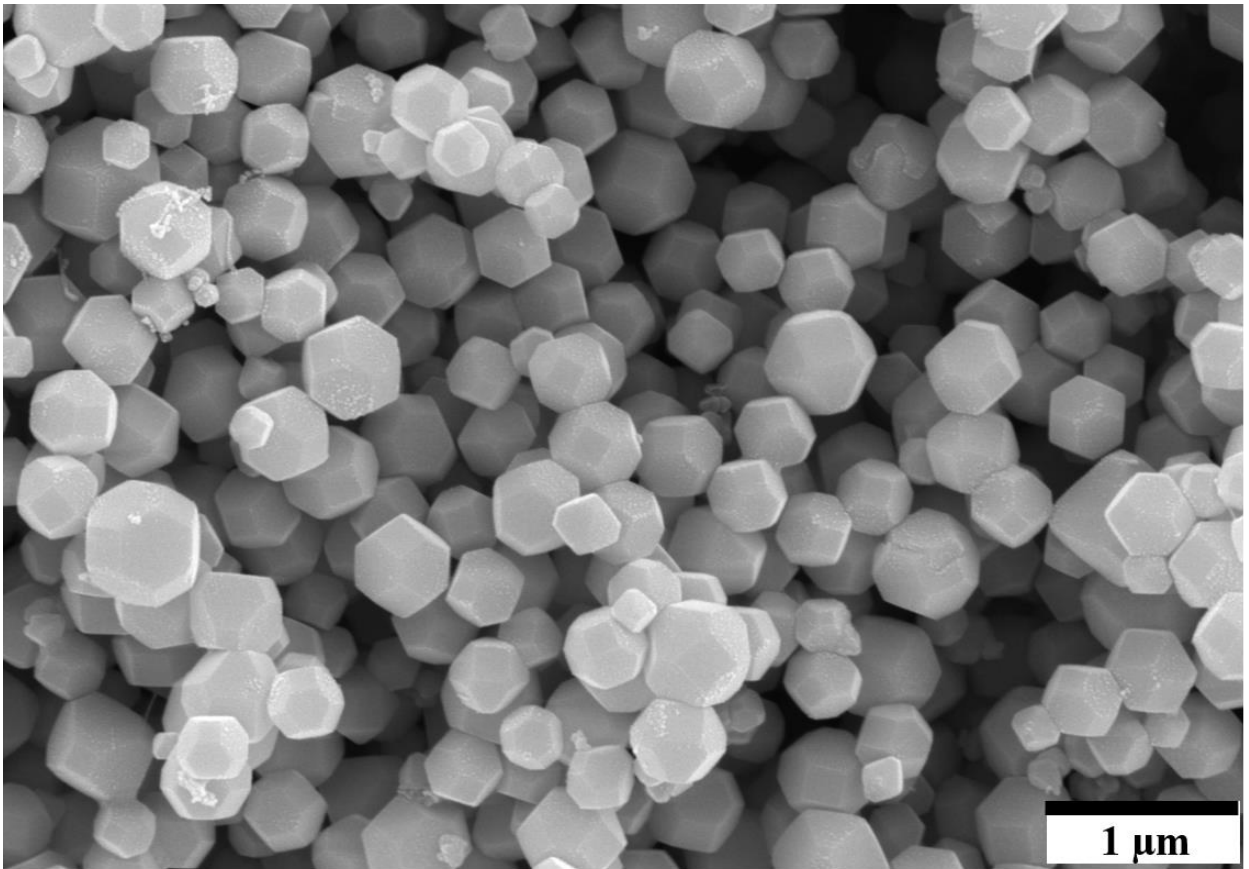


**Figure 11**, SEM image of octahedron Cu<sub>2</sub>O nanoparticle

The as synthesized octahedral nanoparticle Cu<sub>2</sub>O was decorated with Au nanoparticle.

Figure 12, show the SEM image of Au@Cu<sub>2</sub>O octahedral with 500 nm size nanomaterial,

the selective attachment of the Au on octahedral Cu<sub>2</sub>O lattice plane.

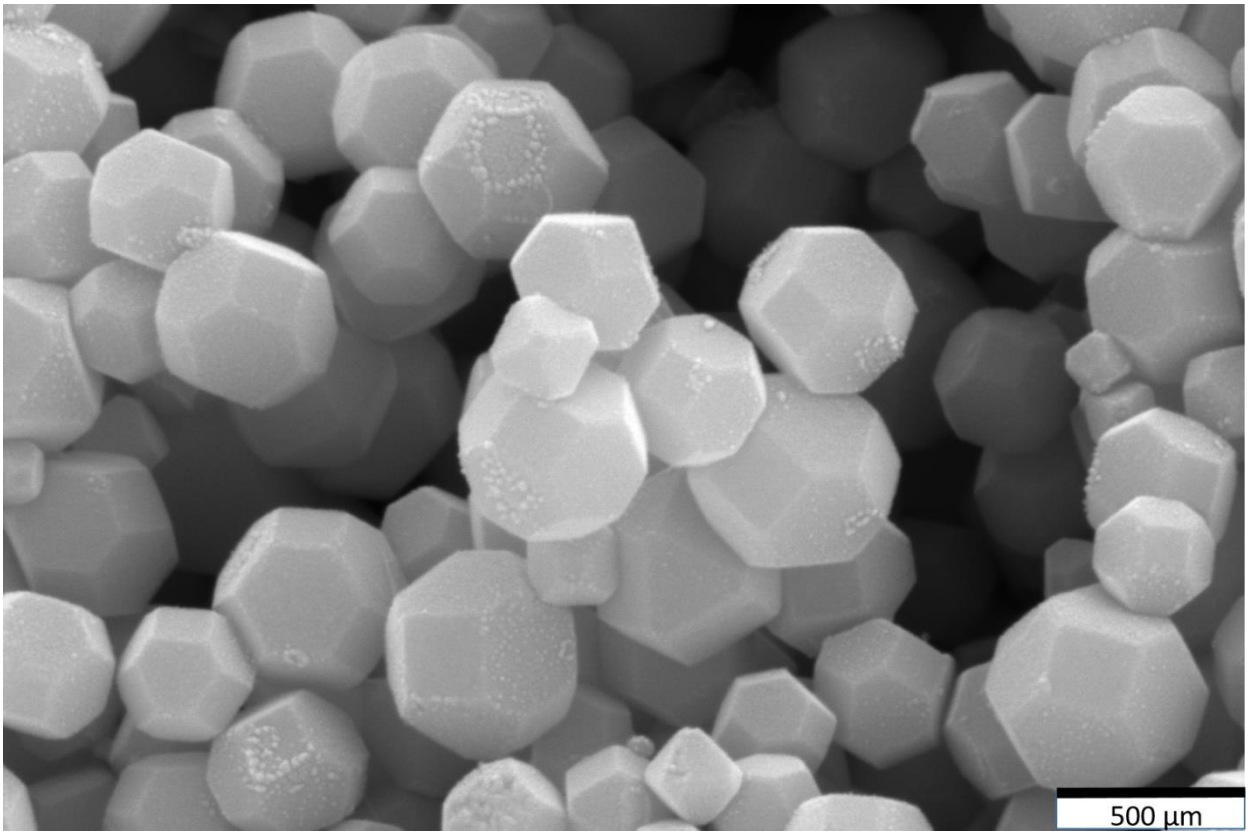


**Figure 12**, SEM image of octahedral Cu<sub>2</sub>O with Au decoration

The selective attachment of the Au is more obvious when the nanomaterial size was 300 μm. Figure 13, present the SEM image of octahedral Cu<sub>2</sub>O with Au deposited at some facet, EDS mapping shown the percentage composition of Au which is 3.8% of the total elemental constituent of the hybrid nanomaterial Au@Cu<sub>2</sub>O. Also the XRD diffractogram correspond to the SEM image where the octahedral lattice plane (110) lack the deposited Au nanoparticle.

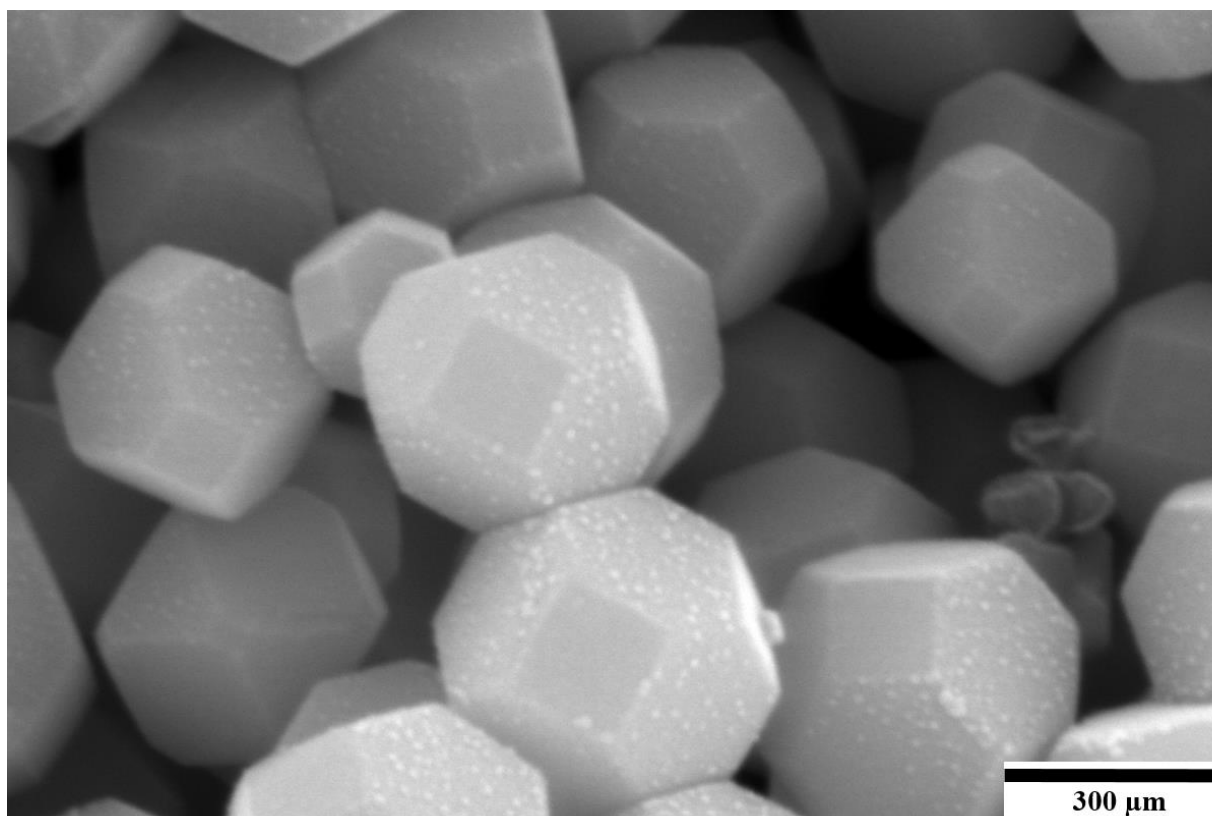


**Figure 13**, SEM image of pristine octahedron Cu<sub>2</sub>O with selective facet Au decoration.

### **4.3 Energy-dispersive X-ray (EDX) Spectroscopy**

Energy – dispersive X-ray spectroscopy (EDX, Oxford-Xmax) enabled us to confirm the elemental composition of the as synthesized nanomaterials. The detected elemental make-up of the nanomaterials is in a good agreement with the data collected and reported by other spectroscopic data (Raman, XRD). Figure 14-16 below shows the percentage composition of the synthesized Cu<sub>2</sub>O nanoparticles and corresponding hybrid nanoparticles with gold and silver for all different morphologies. In Figure 14, the composition make-up of copper and oxygen is shown, the mapping intensity of Cu indicate that it is the most dominant element in the nanoparticle and O<sub>2</sub> is the least dominant. This

can be seen on the graph with Cu taking 89.5% and O<sub>2</sub> constitute 10.5% by the weight. This is in good agreement with the Cu<sub>2</sub>O.

Table 1, the calculated mass ratio of copper and oxygen and percentage composition is reported.

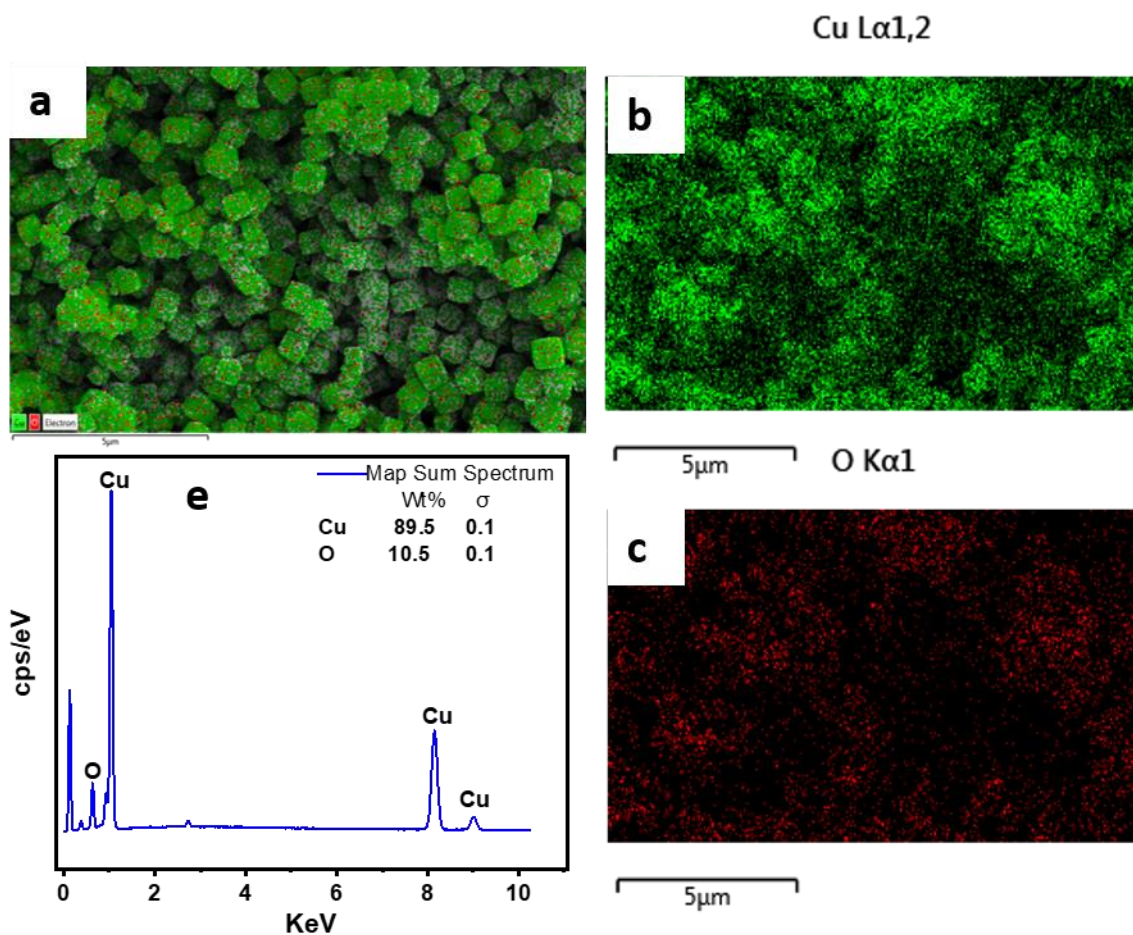


**Figure 14**, EDX mapping of the cube shaped Cu<sub>2</sub>O with the elemental compositions. The SE micrographs, (a) overlay image and (b to c), the EDX mapping of elements Cu & O and (d) EDX spectrum.

The EDX elemental mapping for the gold decorated cube shape Cu<sub>2</sub>O nanomaterial, Figure 15, present the relative elemental amounts that constitute the hybrid nanomaterials. In the EDX image the well synthesized hybrid nanomaterial with uniformity of shape, the Au image is least intense blue color, O image more intense green color and the Cu image is

much more intense red color. Also the table on the graph indicate 83.4% composition of Cu, 16.0% constitute O and Au constitute 0.7 percent of the hybrid nanomaterial. The EDX data graph also show, through the relative intensity of the peak associated to Cu, O and Au. Confirmed the above information on percentage in amount of the element.

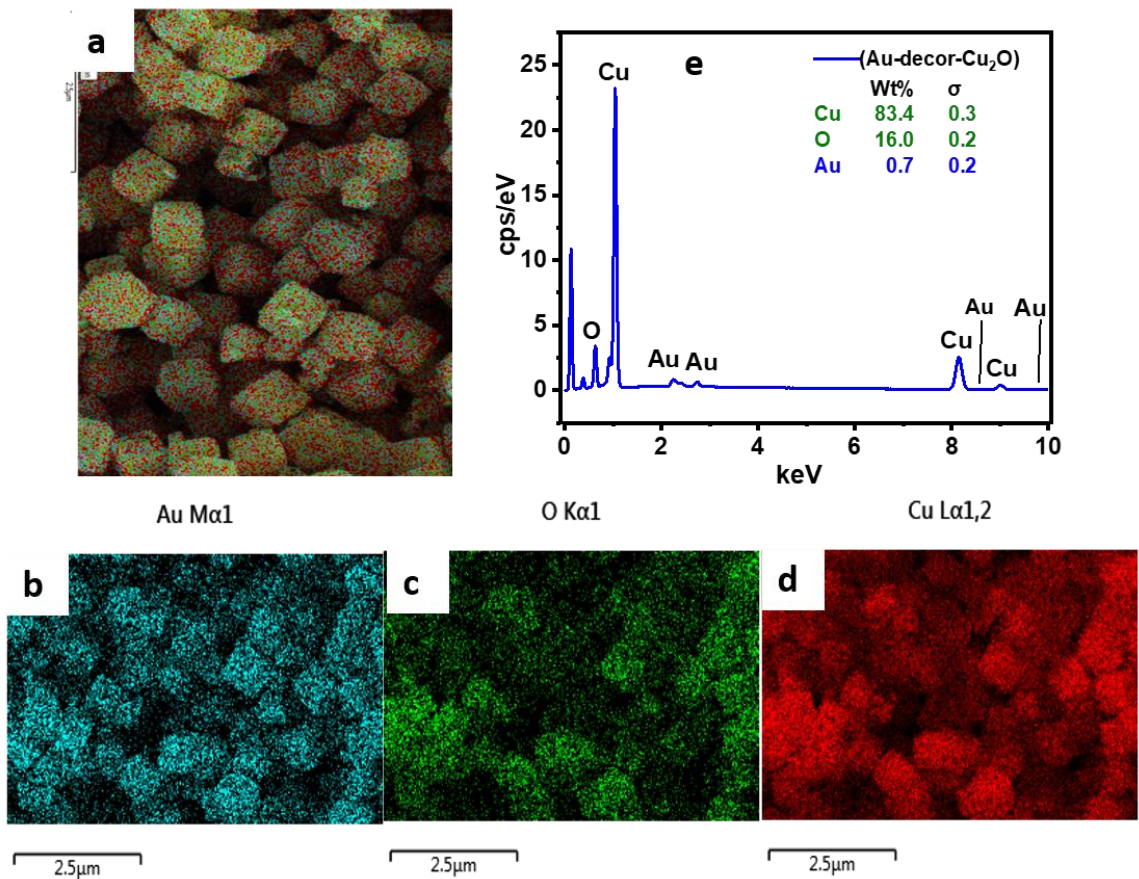


**Figure 15**, EDX mapping of the cube shape Au@Cu<sub>2</sub>O with the elemental compositions. The SE micrographs, (a) overlay image and (b to c), the EDX mapping of elements Cu & O and (d) EDX spectrum

The octahedral shaped Cu<sub>2</sub>O was analyzed using EDX to obtain the comparative percentage composition of each individual element in the hybrid nanomaterials. The image mapping shows the order of intensity varies in intensity from Cu, O, and Au in that other.

The representation in Figure 16 shows, percentage of Au is 3.8% which is more than that present in cube shape morphology, O remain relatively the same 16.0% and Cu reduce to 80.2% from the percentage observed in cubic morphology. The EDX spectrum also present the fact that the image mapping intensity are in agreement.

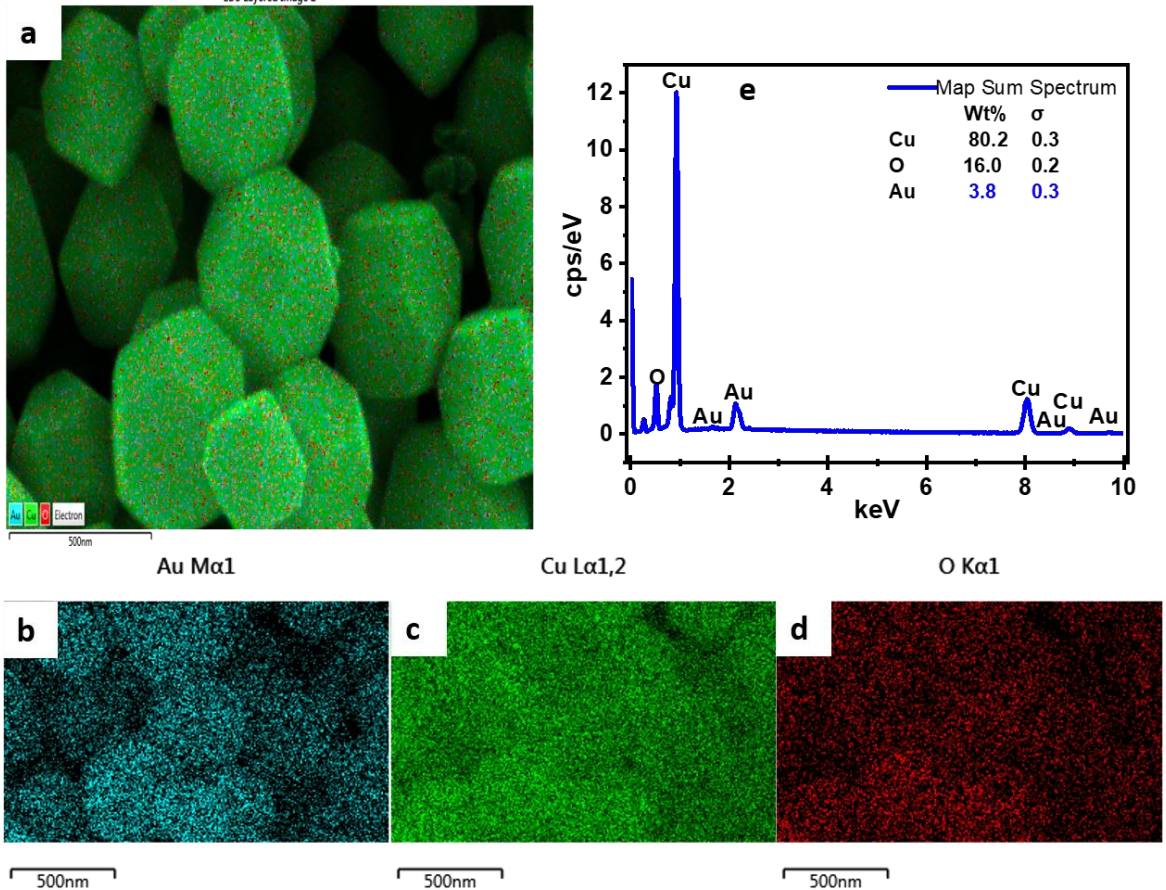


**Figure 16**, EDX mapping of the octahedron shaped Au@Cu<sub>2</sub>O with the elemental compositions. The SE micrographs, (a) overlay image and (b to c), the EDX mapping of elements Cu & O and (d) EDX spectrum.

The nanomaterial synthesized in two shapes of cube and octahedral in the pristine form and the hybridized form, Table 1, present each nanostructure elemental percentage composition and their mass ratio. In the cube Cu<sub>2</sub>O, the Cu percentage is 89.5% and O is 10.5% this agrees with the calculated theoretical mass ratio, while for Au decorated Cu<sub>2</sub>O is compose of 0.7% of Au, 83.4% for Cu and 16.0% of O and their corresponding mass ratio are 0.007:0.833:0.159 respectively. The octahedral Cu<sub>2</sub>O decorated with Au, has 3.8%

of Au, 80.2% of Cu, and 16.0% and the calculated theoretical mass ratio for the hybrid octahedral nanomaterial are 0.038:0.802:0.16.

Nanostructure	Element	Percentage	Mass ratio
Cube Cu <sub>2</sub> O	Cu	89.5	0.896:0.105 ( Cu:O )
	O	10.5	
Cube Au@Cu <sub>2</sub> O	Au	0.7	0.007:0.833:0.1598 (Au:Cu:O)
	Cu	83.4	
	O	16.0	
Octahedral Au@Cu <sub>2</sub> O	Au	3.8	0.038:0.802:0.16 (Au:Cu:O)
	Cu	80.2	
	O	16.0	

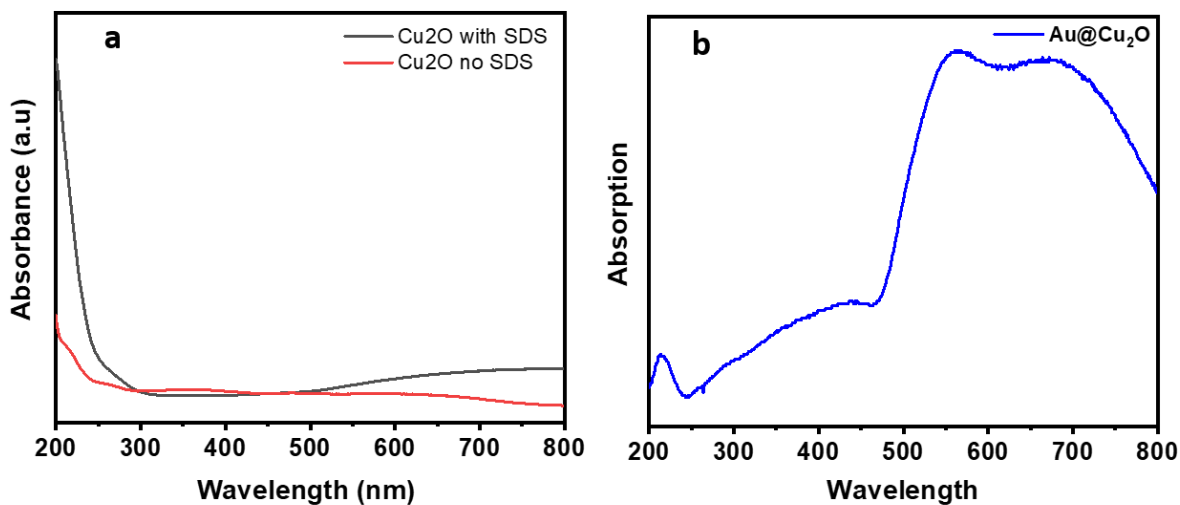
**Table 1,** Show the calculated theoretically, mass ratio of Cu and O in Cu<sub>2</sub>O and the Au, Cu, and O in Au@Cu<sub>2</sub>O

#### 4.4 Ultraviolet-Visible (UV-Vis) Spectroscopy

The ultraviolet and visible (UV-Vis) spectral were measured in range between 0 to 800 nm. The UV-Vis range also stretch the range of human visual sharpness of approximately 400 to 750 nm, which support the spectroscopic usefulness in characterizing the absorption, transmission and reflectivity of the synthesized nanoparticles and the hybrid version. The UV-vis spectra were measured using Genesys 10S UV-Vis spectrometer.

The absorbance observed for Cu<sub>2</sub>O that has been synthesized by adding sodium dodecyl sulfate as surfactant covers more range in the solar spectrum, it shows an absorption from above 800 nm to 530 nm (Figure 1a). In general, Cu<sub>2</sub>O nanoparticles synthesized without SDS show UV-Vis spectra absorption ranging from little bit above 800 nm to 540 nm.

From the observation it can be infer that the surfactant, in this case sodium dodecyl sulfate (SDS) facilitated the formation of nanoparticles with the appropriate orientation, suitable for the efficient visible spectrum. This in return, helps to harvest the maximum portion of solar spectrum which is suitably desired in photocatalytic application. The decoration of the  $\text{Cu}_2\text{O}$  cubes with a plasmonic metal nanoparticles in this case a gold, the resultant UV-Vis spectra shows an increase in the absorbance intensity range of the hybrid nanomaterials from 800 nm to 460 nm (Figure 1b) this reflect the contributive plasmonic property of gold on the semiconductor nanoparticles. Figure 17, (a, b) show the corresponding UV-Vis spectra of the  $\text{Cu}_2\text{O}$  and the hybrid Au- $\text{Cu}_2\text{O}$  nanoparticles.



**Figure, 17** (a) Shows UV-Vis spectra absorption of  $\text{Cu}_2\text{O}$  cube synthesized with and without SDS. (b) Present the UV-Vis spectra of Au decorated  $\text{Cu}_2\text{O}$  cube shaped nanoparticle, with spectra extended up to 460 nm due to the plasmonic contribution of the Au nanoparticle.

The reaction kinetic of the synthesis was monitor through ultraviolet-visible spectroscopy to a full glimpse on the transition stages per minute, illustrating with an Au decorated  $\text{Cu}_2\text{O}$  at 15 min timed interval. The first observed spectra at 15 min, show an absorption at 800

nm only, at 30 min the spectra pattern changes with more absorption at 540 nm and the spectra at 45 min shows high absorption both 540 nm and 800 nm, this is likely due to the nanomaterial formation stages from atoms to cluster and finally to the nanomaterial. Figure 18, give an insight into the nanomaterial formation kinetic mechanism.

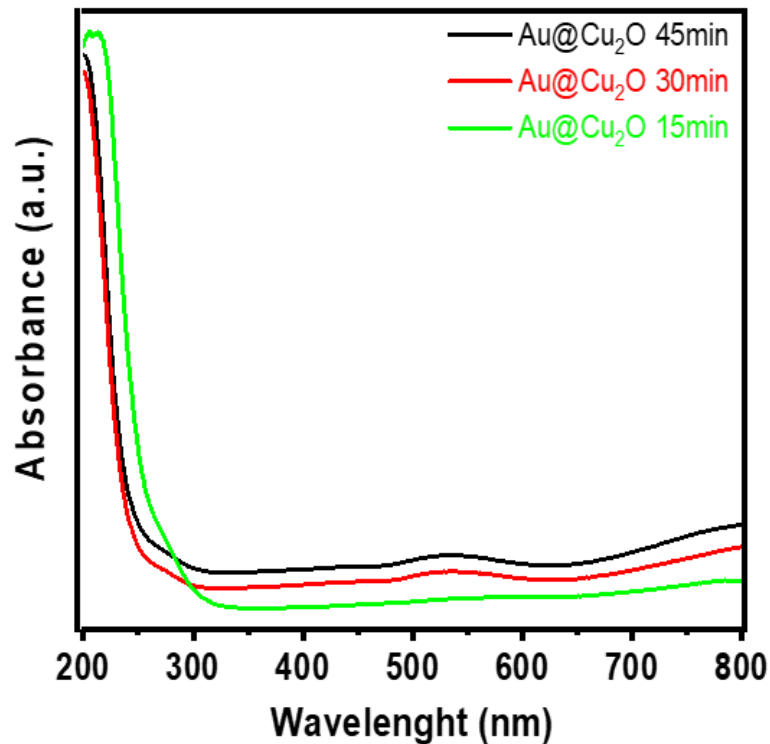


**Figure 18**, showing the sequential change in the absorption upon growth Au domain onto the surface of Cu<sub>2</sub>O cube shape nanoparticles. After 45 minutes, we can clearly see the plasmon band centered at 530 nm. The growth of Au domains has also enhanced the absorption efficiency due to Au-Cu<sub>2</sub>O hybrid nanoparticles.

The UV-Vis spectra for the nanoparticles with morphologies other than cube was also measured using the above stated instrument, the spectra for the octahedral shaped  $\text{Cu}_2\text{O}$  nanoparticle are shown in Figure 19. The washed  $\text{Cu}_2\text{O}$  nanoparticles were analyzed using and UV-Vis spectra were measured Figure 19a. The spectrum indicated an absorbance at 800 nm to 650 nm. The Figure 19b represent the effect of the introduced gold on the visible light absorbance of the octahedral shaped  $\text{Cu}_2\text{O}$  with Au nanomaterial. It showed strong absorption in the visible region and a distinctive Plasmon band centered at 520 nm due to the presence of Au nanoparticles. Overall, the  $\text{Cu}_2\text{O}$  with octahedron shape decorated with Au showed better absorption the visible range than alone  $\text{Cu}_2\text{O}$ .

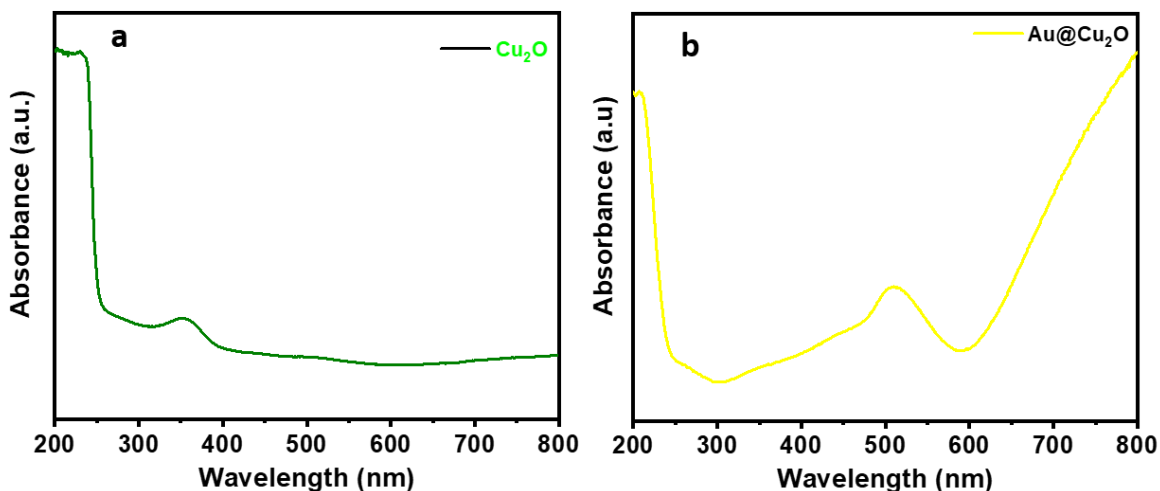


**Figure 19,** (a) A UV-Vis-Spectra of the as synthesized octahedral  $\text{Cu}_2\text{O}$ , showing absorption at 800 nm till 650 nm, (b) A very high intense absorbance peak around 800 nm which can be attributed to  $\text{Cu}_2\text{O}$  and another peak extension at 520 nm assumed to be as a result of the plasmon effect of the Au nanoparticle.

## 4.5 RAMAN Spectroscopy

Raman spectra were measured on iH320 Horiba spectrometer with charge-coupled device (CCD) using monochromatic laser (300mW, 532nm), grating of  $1200\text{cm}^{-1}$  and an aluminum substrate. Raman spectroscopy furnish chemist with the information on the crystal structure of the synthesized nanoparticle and hybrid nanomaterial in this case  $\text{Cu}_2\text{O}$  and Au nanoparticles decorated  $\text{Cu}_2\text{O}$ . The  $\text{Cu}_2\text{O}$  and Au- $\text{Cu}_2\text{O}$  cube and octahedral morphology were characterized using Raman spectroscopy, they exhibit a characteristic Raman bands at  $218\text{cm}^{-1}$ ,  $523\text{cm}^{-1}$  and  $623\text{cm}^{-1}$ . These correspond to characteristic Raman Band for the  $\text{Cu}_2\text{O}$  as reported earlier by Yilin Deng on Raman spectroscopy study of copper oxide during electrochemical oxygen evolution reaction. The Raman spectra of the pristine  $\text{Cu}_2\text{O}$  and the Au doped  $\text{Cu}_2\text{O}$  are shown in Figure 20 (a, b) below.

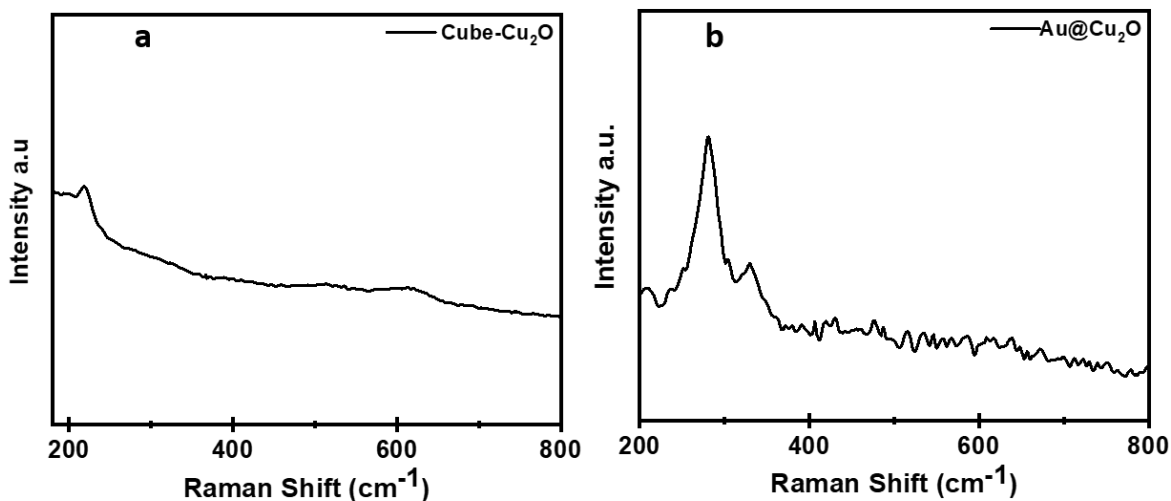


**Figure 20**, In (a) Raman shift pattern at  $218\text{cm}^{-1}$  and  $623\text{cm}^{-1}$  was present which were due to  $\text{Cu}_2\text{O}$  cube, (b) shows Raman band at  $218\text{cm}^{-1}$ ,  $523\text{cm}^{-1}$  and  $623\text{cm}^{-1}$ , the high intensity band at  $218\text{cm}^{-1}$  and the observed band at  $523\text{cm}^{-1}$  resulted from the Au hybridized  $\text{Cu}_2\text{O}$ .

The Raman characterization of octahedral morphology is represented in figure 5 for both the pristine octahedral and the Cu<sub>2</sub>O decorated with Au. The octahedral Cu<sub>2</sub>O shaped nanoparticle on the show (Figure 21a) a strong Raman band at 218cm<sup>-1</sup> and low band at 623cm<sup>-1</sup> and when the octahedral Cu<sub>2</sub>O (Figure 21b) is decorated to Au, Raman band was observed at 218 cm<sup>-1</sup>, 523 cm<sup>-1</sup> and 623 cm<sup>-1</sup>. A unique band at 260 cm<sup>-1</sup> which also give more credence to the Au deposited on the Cu<sub>2</sub>O.

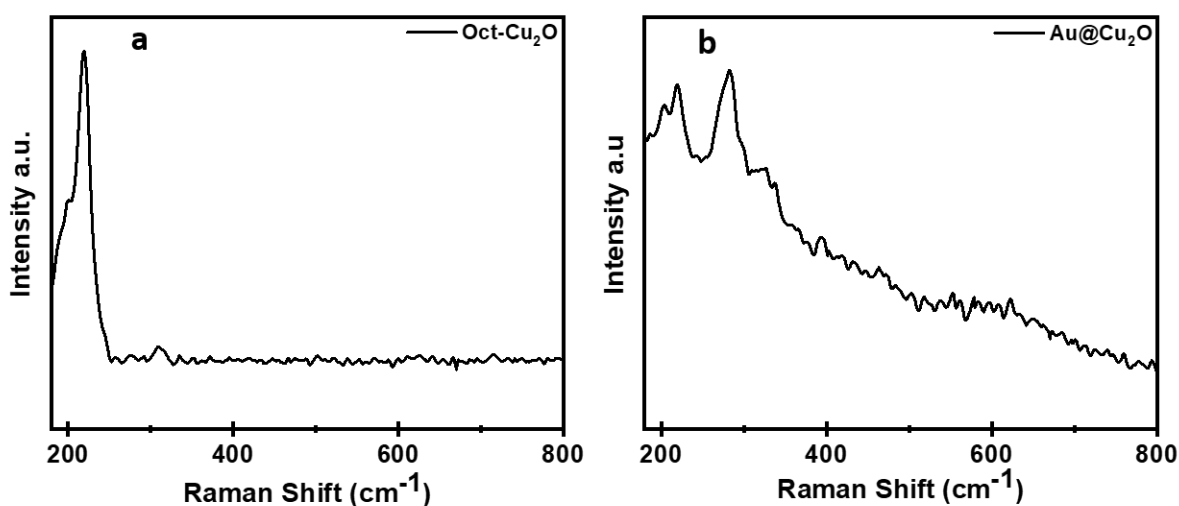


**Figure 21**, (a) Raman band of octahedron Cu<sub>2</sub>O is presented with intense band at 218<sup>-1</sup> with less obvious band at other Raman shift, which is attributed to the morphology of the pristine nanoparticle, (b) Shows the plasmon resonance contributive effect of Au on pristine octahedron Cu<sub>2</sub>O, with the 260 cm<sup>-1</sup> in addition to 523 cm<sup>-1</sup> and 623 cm<sup>-1</sup> band been due to Au decorative effect on Cu<sub>2</sub>O.

#### 4.6 X-ray Diffraction (XRD)

The patterns of the X-ray diffraction were measured using the Rigaku Miniflex II instrument with a monochromator CuK $\alpha$ 1 (1.5406Å) at 30kV, 15mA. The XRD patterns were recorded in the static scanning mode from (2 $\theta$ ) 20<sup>0</sup> to 80<sup>0</sup> at a detector angular speed

of  $4^{\circ}\text{min}^{-1}$  and step size of  $0.02^{\circ}$ . The arrangement of atoms in a solid can be elucidated with aid of XRD. The distance between atoms in a lattice is approximately equivalent to the wavelength of the X-rays, when the beam of X-rays radiation falls on a crystal, the resultant deflection by the crystals are captured by a photographic plate which is obtain as an output. It is a technique used to examine the morphological crystal structure of the synthesized  $\text{Cu}_2\text{O}$  and  $\text{Au-Cu}_2\text{O}$  based nanoparticles. In Figure 22, pristine Copper oxide synthesized without SDS and with SDS is shown with diffractograms having reflections at  $(2\theta)$   $29^{\circ}$ ,  $37^{\circ}$ ,  $43^{\circ}$ ,  $61^{\circ}$ ,  $74^{\circ}$ , and  $77^{\circ}$ . The diffraction reflection at  $29^{\circ}$  is attributed to the (110) facet of  $\text{Cu}_2\text{O}$ , that at  $37^{\circ}$  is associated to a  $\text{Cu}_2\text{O}$  nanoparticle with a facet of (111), diffraction reflection at  $43^{\circ}$  correspond to (200), while the facet (220) is in tendon with  $61^{\circ}$ . Also the diffraction reflection at  $74^{\circ}$  and  $77^{\circ}$  correspond to the facet (311) and (222) respectively.

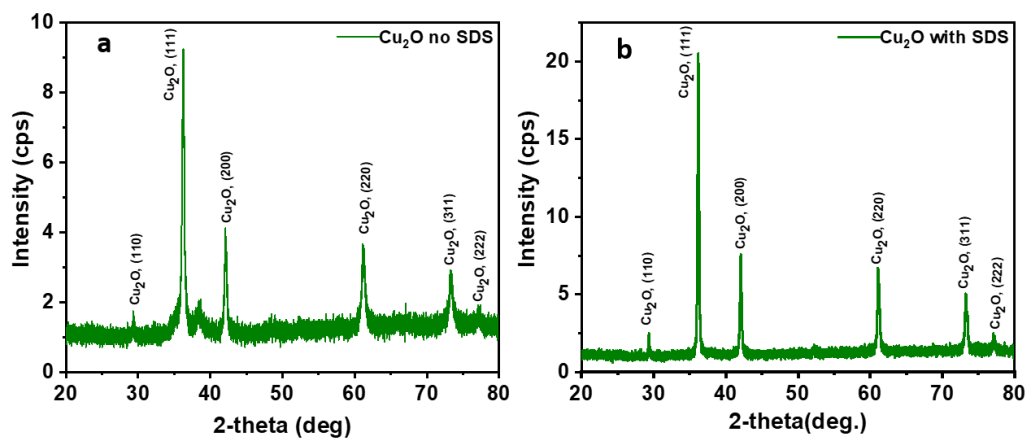


**Figure 22,** (a) XRD diffractogram of as synthesized  $\text{Cu}_2\text{O}$  without the use of a surfactant (SDS), extra reflection in the pattern at  $37^{\circ}$  could be due to impurity  $\text{CuO}$ . (b) Shows the XRD pattern for a  $\text{Cu}_2\text{O}$  synthesized using surfactant (SDS), all the reflections in the diffractogram

matches well with the  $\text{Cu}_2\text{O}$  ( $\text{Pn}\bar{3}\text{m}$ ). This confirms the phase purity of as synthesized  $\text{Cu}_2\text{O}$  nanocubes.

The XRD diffractogram of the as synthesized cube shape  $\text{Cu}_2\text{O}$  semiconductor nanoparticle decorated with noble metal (Au) were investigated to ascertain the contributive effect of the Au on the crystal structure of the  $\text{Cu}_2\text{O}$  semiconductor. Figure 23, here below, present the unique XRD pattern of the hybrid nanomaterial between  $\text{Cu}_2\text{O}$  and Au. The very obvious diffraction reflections at  $38^\circ$  and  $77^\circ$  shows the presence of Au domains with the facet (111) and (311) respectively.

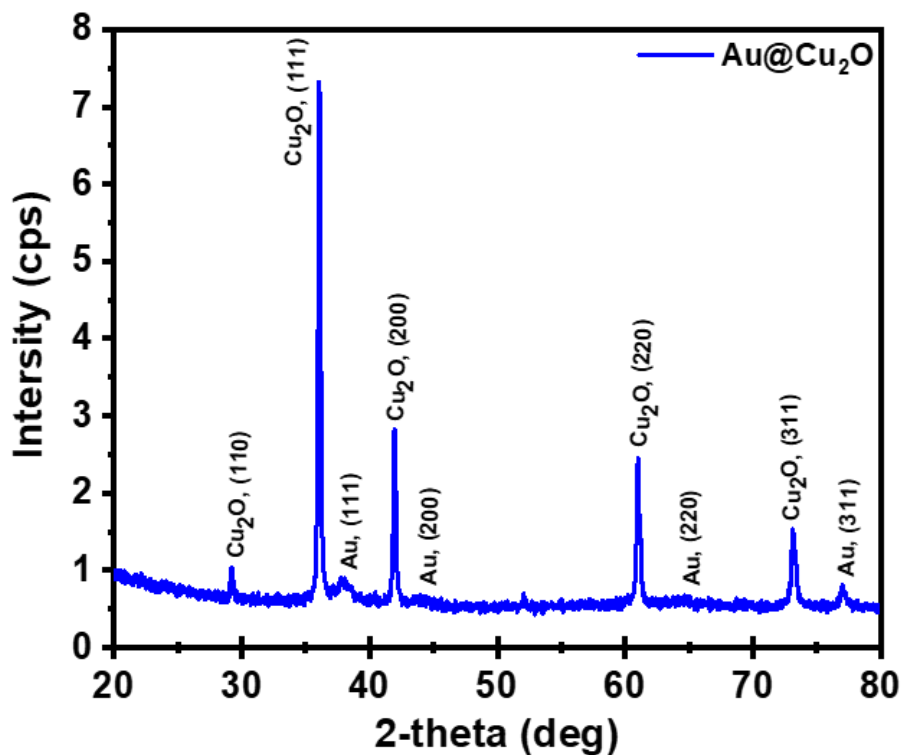


**Figure 23**, Show the XRD diffractogram of cube shape  $\text{Cu}_2\text{O}$  decorated with Au nanoparticles.

The XRD pattern of the  $\text{Cu}_2\text{O}$  nanoparticles with octahedral morphology was also investigated using the same instrument as stated above under similar set of conditions. The diffraction pattern is shown in Figure 24. The all reflection could be indexed to phase pure  $\text{Cu}_2\text{O}$  with space group (here write space group). All the reflection observed can be easily indexed to octahedron lattice phase

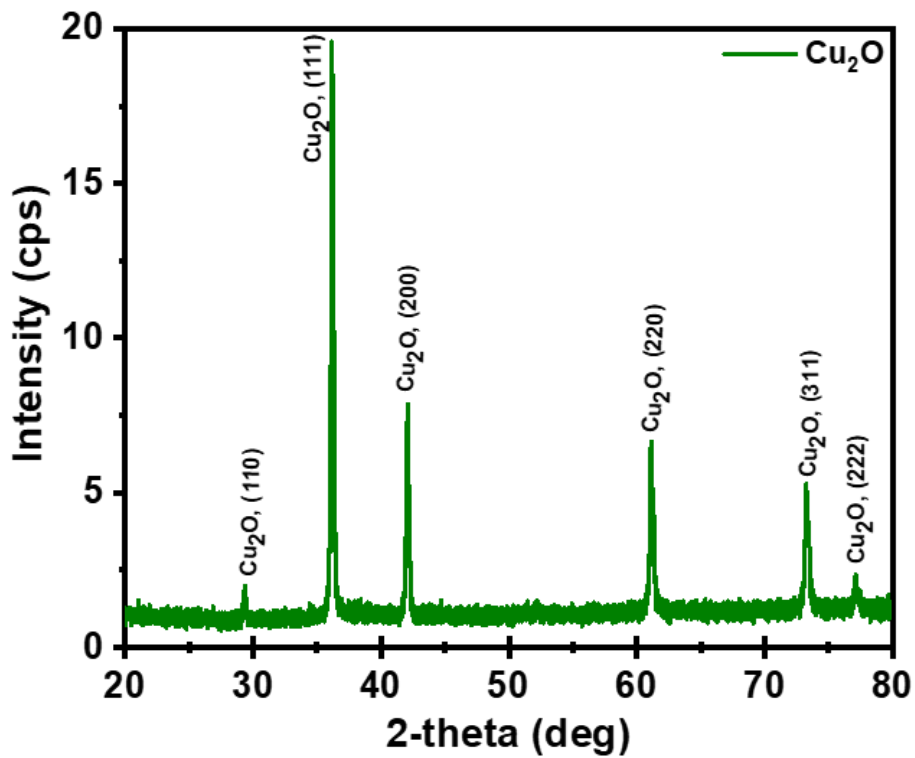


**Figure 24**, Represent the XRD diffractogram of octahedral shaped  $\text{Cu}_2\text{O}$ ,

Furtherance to the XRD pattern observed with the octahedron shape  $\text{Cu}_2\text{O}$  that is not a hybridized with Au nanomaterial, the crystal structure of the hybridized nanomaterial was measured to obtain the crystal structural contribution of the newly introduced Au nanoparticle on the semiconductor nanoparticle. The pattern of the octahedral nano-

structure  $\text{Cu}_2\text{O}$ , decorated with Au is detailed in Figure 25. The purity of the nanomaterial was attested by the fact that the diffraction pattern shows no any extra diffraction other than the expected pattern, usually when extra pattern is present that suggest the presence of impurity in the synthesized nanomaterial. This claim is further confirmed from the EDX analysis, as the elemental mapping only present the element of copper and oxygen in case of pristine  $\text{Cu}_2\text{O}$  and Au, Cu and oxygen for hybrid nanomaterials.

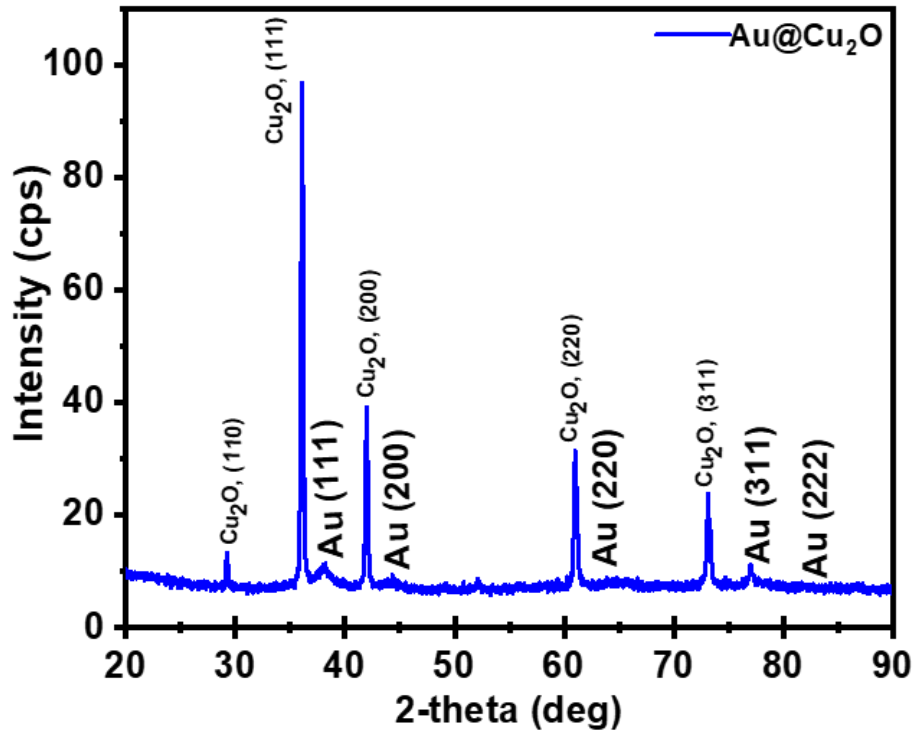
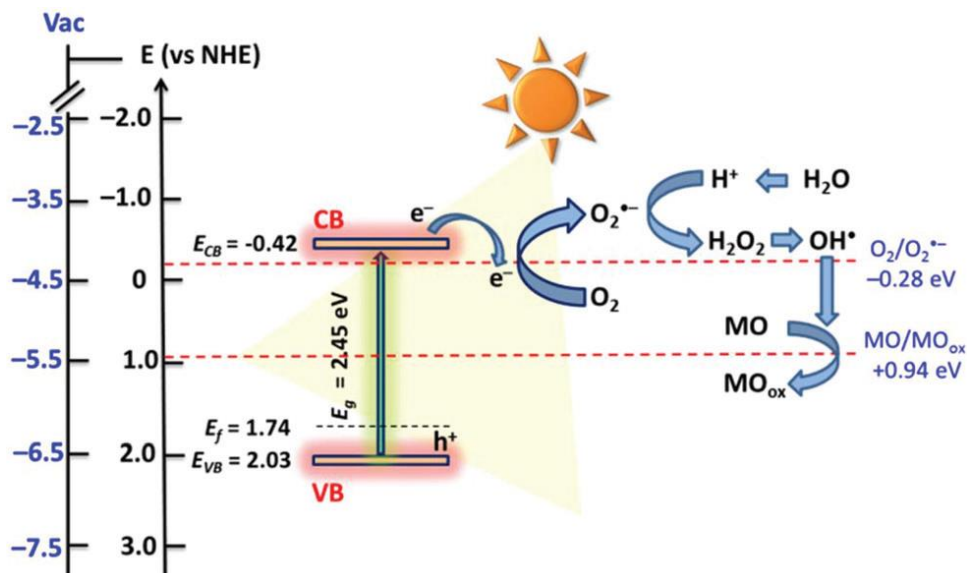


**Figure 25**, Show the diffractogram of octahedral  $\text{Cu}_2\text{O}$  with some Au deposition on selected facet.

## 4.7 Photocatalytic Application

The surface engineered hybrid nanoparticles are used for visible light assisted photo-catalysis for the degradation of organic pollutants in water. The size, composition and surface area of nanomaterial plays a crucial role in photocatalytic applications. The energy of the surface site depends on particle size, shape and surface chemistry. The catalytic activity is enhanced when the physical properties of the surfaces are improved by the introduction of novel noble metal to a pristine  $\text{Cu}_2\text{O}$ . The pristine  $\text{Cu}_2\text{O}$  and Au decorated  $\text{Cu}_2\text{O}$  of cube shape and octahedral morphology were evaluated for photocatalytic activities as a photo-degradation of methylene blue (ME) dye under visible-light irradiation. The analysis procedure entails prior to the exposure to visible light radiation,  $5 \times 10^{-5}$  M of the ME dye solution, prepared by adding 2mg of dye in 20ml of  $\text{H}_2\text{O}$  and 2mg of the nanomaterial was added into the ME solution in the absence of light, and left for 30 min to ensure equilibrium is established between the ME and the nanomaterials. The pristine methylene blue (ME) shows a strong absorption peak at 670 nm wavelength, and the photo-degradation on the addition of nanomaterial was monitored by evaluating the decrease in absorbance intensity using ultraviolet-visible spectroscopy at interval of 15 min<sup>52-55</sup>. Here in Scheme 10, is the schematic energy representation of band gap diagram of  $\text{Cu}_2\text{O}$  nanoparticles, that illustrate their ability to be photoexcite through the aid of visible light to generate  $\text{OH}^\cdot$  radicals which can participate actively in the photo-oxidation ME molecules.



**Scheme 10**, Represent band gap of  $\text{Cu}_2\text{O}$

Cube shape pristine  $\text{Cu}_2\text{O}$  with ME analyzed with UV-Vis Spectroscopy, indicate small decrease in absorbance intensity as the measurement time increases from 0 min to 45 min, this is shown in figure 26.

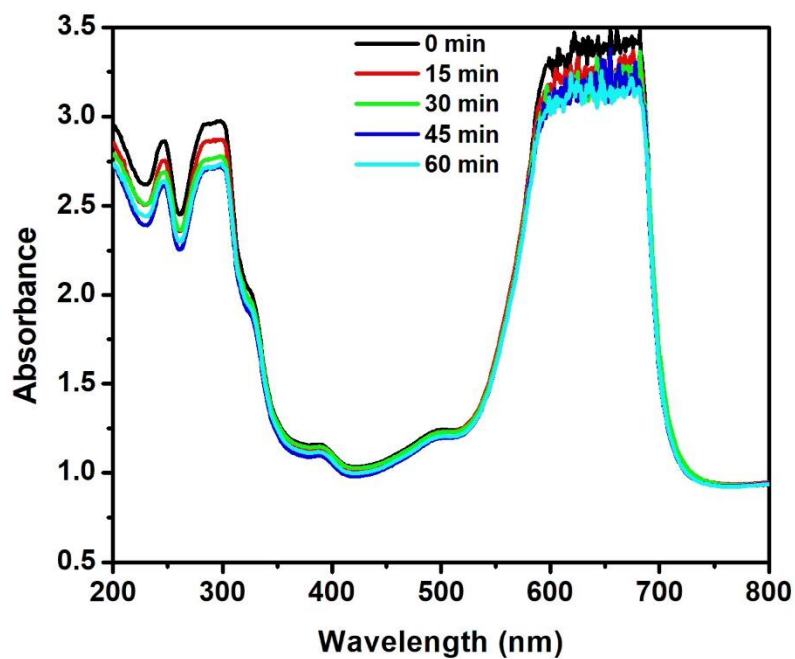


**Figure 26**, Photo-degradation of methylene blue on Pristine  $\text{Cu}_2\text{O}$  at 15 min interval.

The UV-Vis spectra of the Au decorated Cu<sub>2</sub>O with cube morphology, Figure 27, indicate a sharp decrease in the degradation of methylene blue (ME), for much more than when the undecorated Cu<sub>2</sub>O were used for the same purpose at the same time interval. At 0 min of taking the UV-Vis measurement, the peak intensity is 3.5 at 670 nm, after 15 min of exposure to the full visible spectrum range the photo-degradation of ME is at an average of 0.4 absorbance decrease.

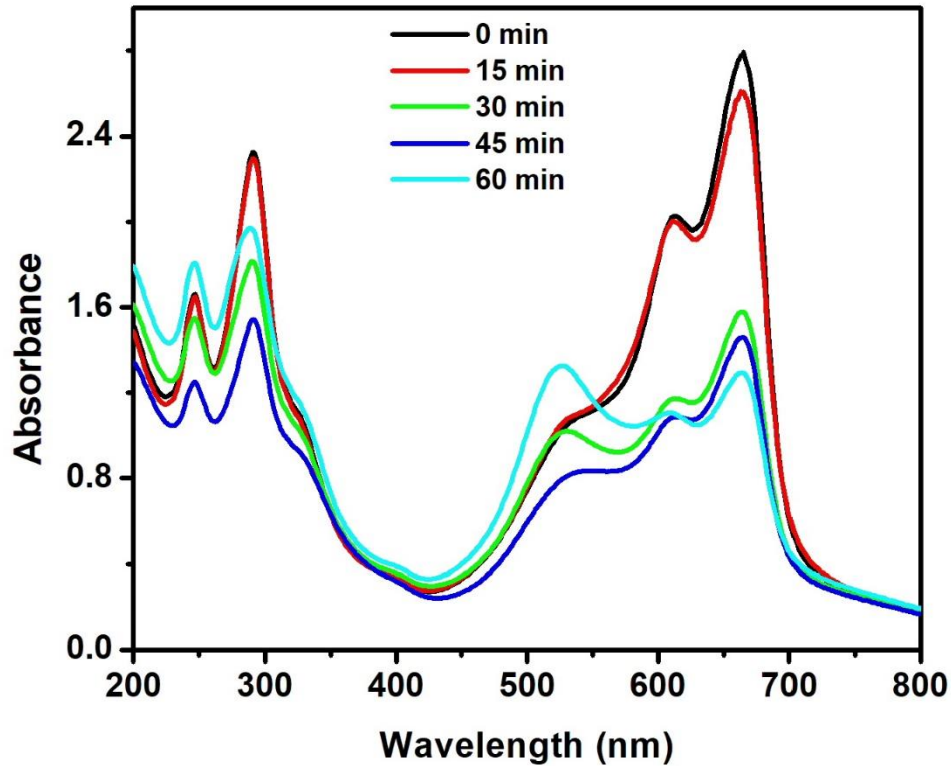


**Figure 27**, Au-Cu<sub>2</sub>O hybrid photo-degradation of ME

In the case of the  $\text{Cu}_2\text{O}$  nanoparticles with octahedron morphology, the UV-Vis spectroscopy measurement for evaluating the photo-degradation of solution of ME, depict an absorbance which does not decrease much with the 15 min time interval set for observing the photo-degradation power of the octahedral  $\text{Cu}_2\text{O}$  morphology, from the graph it can be infer that at every 15 min only about 0.1 absorbance is lost, and this implies that the nanomaterial only degrades ME at a slow rate. In figure 28, ten (10) UV-Vis spectroscopy measurement was taken and the absorbance interval was uniform.

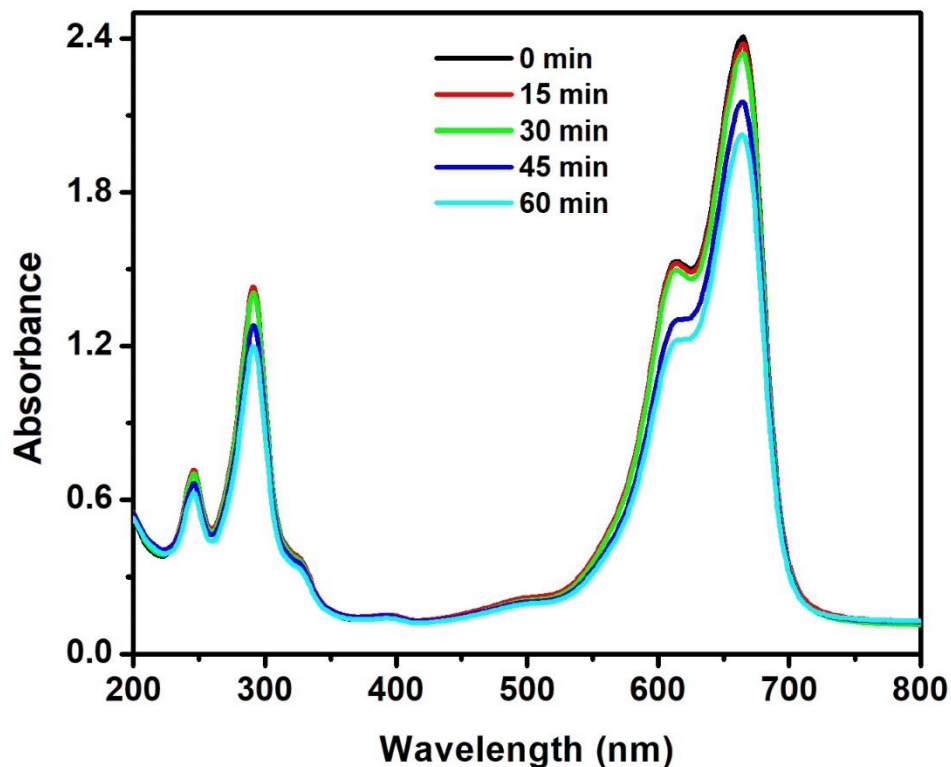


**Figure 28**, ME degradation by octahedral  $\text{Cu}_2\text{O}$

There was a great departure in the photo-degradation activity of Cu<sub>2</sub>O decorated with Au, as compare to the pristine Cu<sub>2</sub>O. here, starting from the measurement at 0 min, and the second measurement at 15 min that absorbance difference was very small, that means that for 15 min only small percentage was degraded, beyond 15 min there was a shape photo-degradation of ME which signifies the contributive effect of the Au to the photocatalytic performance of the nanomaterial and this is shown in figure 29.

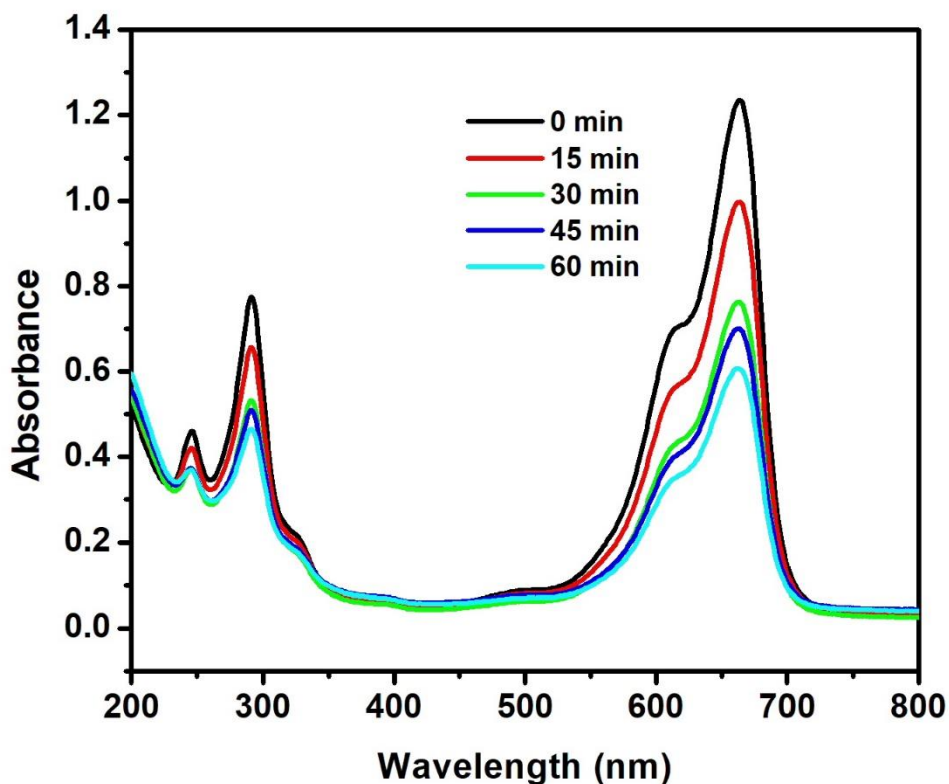


**Figure 29**, Octahedral Au decorated Cu<sub>2</sub>O photo-degradation of ME

In other to understand the kinetic that governs the photocatalytic degradation of organic pollutant in water, the pseudo-first-order model was a suitable model that is generally used to express the photo-degradation process with an initial concentration been low. This is expressed in equation 1.

$$\ln\left(\frac{C_0}{C}\right) = kt \quad (1)$$

Where  $C_0$  is the initial concentration and  $C$  is the concentration at time ( $t$ ),  $k$  represents the pseudo-first order rate constant and  $t$  stand for time. Figure 30, present the comparative kinetics photocatalytic methylene blue degradation by independent pristine cubic and octahedron  $\text{Cu}_2\text{O}$  morphology as well as their hybridized nanoparticle with gold,  $\text{Au@Cu}_2\text{O}$ . It becomes more clear that the Au hybrid result in some enhanced photocatalytic properties of the as synthesized nanomaterial. For the pristine cubic  $\text{Cu}_2\text{O}$  only about 10% degradation of methylene blue was achieved at 60 min of degradation time, why for octahedron 12% degradation at same 60 min. The degradation power of the nanomaterial increased to 38% and 45% for cubic and octahedron  $\text{Au@Cu}_2\text{O}$  respectively.

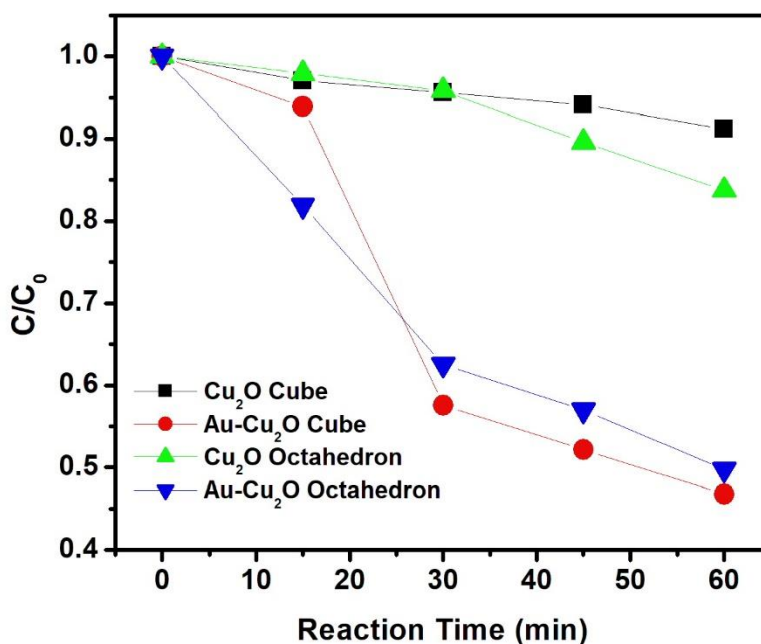


**Figure 30**, Photocatalytic degradation kinetic of methylene blue in water in two  $\text{Cu}_2\text{O}$  morphology and their hybridized  $\text{Au@Cu}_2\text{O}$ .

## CHAPTER 5

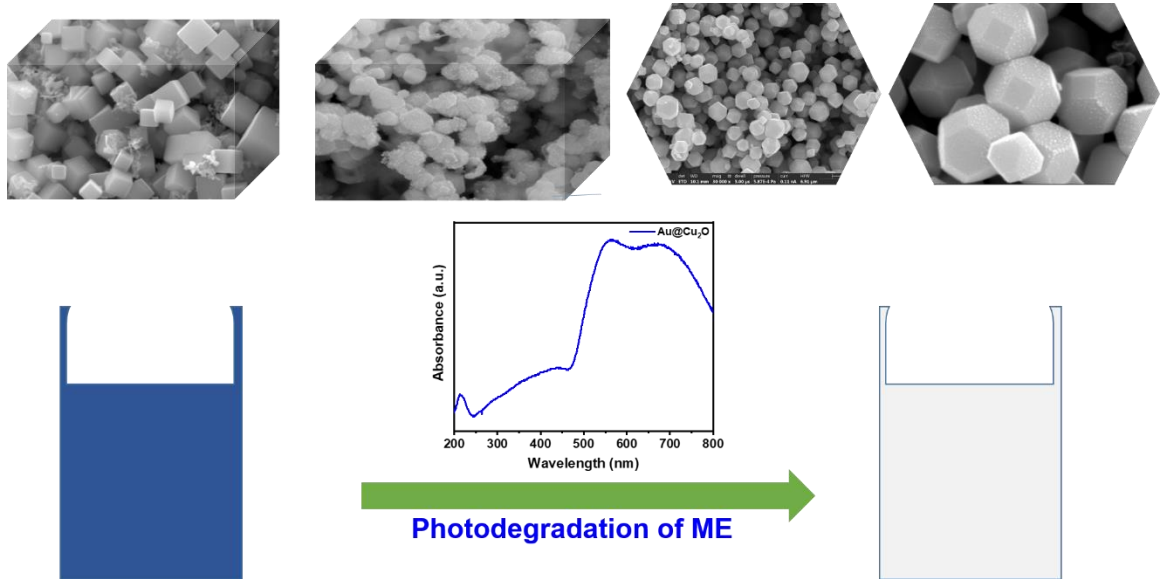
### CONCLUSION AND RECOMMENDATIONS

In conclusion, the synthesis of Cu<sub>2</sub>O nanomaterials with different morphologies and their corresponding hybridization with Au to synthesize hybrid nanomaterials is successfully carried out. The different pristine as well as hybrid materials were characterized using different analytical techniques. The photocatalytic application result showed enhanced activity for the hybrid nanomaterials. Here the outcome is summarized;

1. Cubic Cu<sub>2</sub>O nanoparticle was successfully synthesized using sonication after month of attempt on using non aqueous method to synthesis cubic Cu<sub>2</sub>O and then unfold the possibility of making out other morphology from the main cubic target by adjusting the synthesis conditions to actualize the shapes such as rhombic, octahedral etc. In the non-aqueous approach synthesis, ethylene glycol was employed as the reaction medium, copper acetate was use as the precursor salt in the while glucose was used as reducing agent. The non-aqueous approach was jettison as it continues to be so difficult to achieve the end target, judging by the color that is observed as against the expected color of yellow orange, probably due to the inability to mimic the pre-existing synthesis procedural condition.
2. In a novel approach, we were able to synthesis Cu<sub>2</sub>O within an aqueous medium and functionalized this semiconductor material for photostability and effective, efficient visible light harvesting which could be used for pollutant degradation, organic synthesis, water splitting and in the reduction of CO<sub>2</sub>. Although, we focus the

application of the an-synthesis nanomaterial on water purification with hope to explore it usefulness in the other above stated areas in the future.

3. The visible light harvesting is test for pristine and hybrid  $\text{Cu}_2\text{O}$  reflect the contributive plasmon metal effect on the semiconductor. When the nanomaterial was added into water contaminated with methylene blue (ME), the hybrid nanomaterial for the two morphology investigated show a greater degradation power as compare to the pristine semiconductor.



## **RECOMMENDATION**

The following are recommended for future work

1. The large scale synthesis of  $\text{Cu}_2\text{O}$  for industrial application.
2. Commercialization of gold decorated  $\text{Cu}_2\text{O}$  hybrid nanomaterial.
3. Application of the  $\text{Cu}_2\text{O}$  nanoparticle for anti-bacterial infection

## References

- 1 Wood G. **2020**, Fossil Fuels in a Carbon-Constrained World. In: Wood G., Baker K. (eds) *The Palgrave Handbook of Managing Fossil Fuels and Energy Transitions*. Palgrave Macmillan, Cham
- 2 I. Roger, M. A. Shipman and M. D. Symes, *Nat. Rev. Chem.*, **2017**, 1, 0003.
- 3 C. L. Muhich, B. D. Ehrhart, V. A. Witte, S. L. Miller, E. N. Coker, C. B. Musgrave and A. W. Weimer, *Energy Environ. Sci.*, **2015**, 8, 3687.
- 4 P.V. Kamat, and J. Bisquert, *J. Phys. Chem., C* **2013**, 117, 14873.
- 5 J.C. Colmenares, and R. Luque. *Chem. Soc. Rev.*, **2014**, 43, 765.
- 6 W.C.J. Ho, Q. Tay, H. Qi, Z. Huang, J. Li, and Z.Chen, *Molecules* **2017**, 22, 677.
- 7 International Energy Agency. Key World Energy Statistics; **2014**.  
<https://www.iea.org/fuels-and-technologies>
- 8 N.S Lewis, and D.G Nocera, *Proc. Natl. Acad. Sci. U. S. A.* **2006**, 103, 15729.
- 9 Lolz Etgar, *Materials* **2013**, 6, 445
- 10 W. Zhang,R.Wang, H. Wang and Z. Lei. *Fuel Cells* **2010**, 10, 734
- 11 T.D. Schladt, M.I. Shukoor, K. Schneider,M. N Tahir, F. Natalio, I. Ament, J. Becker, F.D. Jochum, S. Weber, O. Kohler, P. Theato, L.M. Schreiber, C. Sonnichsen, H.C. Schronder, W.E.G. Muller, and W. Dremel. *Angewandte Chemie* **2010**, 49,3976,
- 12 G. Liao, S. Chen, X. Quan, H. Chen, and Y. Zhang *Environmental Science & Technology* **2010**, 44, 3481.
- 13 U.I GayaA.and H. Abdullah *J Photochem Photobiol*, **2008**, 9, 1.
- 14 G. Yang D. Chen H. DingJ. Feng, J.Z. Zhang, Y. Zhu, S. Hamid, and D.W. Bahnemann. *Appl Catal B Environ.* **2017**, 219, 611.
- 15 Y. Bessekhoad, D. Robert and J.V. Weber *J Photochem Photobiol, A* **2004**, 163,569.

- 16 D. Chen, Z. Wang, T. Ren, H. Ding, W. Yao, R. Zong, and Y. Zhu . *J Phys Chem C* **2014**, *118*, 15300.
- 17 L. Jiangtian, K. Scott, Cushing, J. Bright, F. Meng, R. Tess, Senty, P. Zheng, A. D. Bristow, and N. Wu *ACS Catalysis* **2013**, *3*, 47.
- 18 Y.A.Wu, I. McNulty, C. Liu, K.C. Lau, Q. Liu, A.P. Paulikas, C. Sun, Z. Cai, J. R. Guest, Y. Ren, V. Stamenkovic, L.A. Curtiss, Y. Liu, and T. Rajh. . *Nat Energy* **2019**, *4*, 957.
- 19 P.K. Pagare, and A.P. Torane, *Microchim Acta*. **2016** *183*,2983.
- 20 A.F. Wright, and J.S. Nelson, . *J. Appl. Phys.* **2002**, *92*, 5849.
- 21 R. Wick and S. D. Tilley. *The Journal of Physical Chemistry C* **2015**, *119*, 26243.
- 22 Z. Chen, T.F. Jaramillo, T.G. Deutsch, A. Kleiman-Shwarsctein, A. F. Forman, N. Gaillard, R. Garland, K. Takanabe, C. Heske, M Sunkara, E.W. McFarland K. Domen, E. L. Miler, J.A. Turner and H. N. Ding.. *J. Mater. Res.* **2010**, *25*, 3.
- 23 M. Staniuk, D. Zindel, W. van Beek, O. Hirsch, N. Kränzlin, M. Niederberger and D. Koziej, *CrystEngComm*, **2015**, *17*, 6962.
- 24 M. N. Tahir, F. Natalio, M. A. Cambaz, M. Panthofer, R. Branscheid, U. Kolb, W. Tremel, M. Panthofer, R. Branscheid, U. Kolb and W. Tremel, *Nanoscale*, **2013**, *5*, 9944.
- 25 Lolz Etgar, *Materials* **2013**, *6*, 445
- 26 J.S. Sekhon., and S.S. Verma, *Plasmonics*, **2011**, *6*, 311.
- 27 B. Akanksha, and S. Verma, *Optics Communications*, **2019**; *452*; 264.
- 28 K Lee M. and El-Sayed *J Phys Chem B* **2006**, *110*, 19220.
- 29 P.K. Pagare, and A.P. Torane, *Microchim Acta* **2016** *183*,2983.
- 30 J. Lu, J. Xing, D. Chen, H. Xu, X. Han, and D. Li, *J Mater Sci* **2019**, *54*, 6530.
- 31 <http://www.mindat.org/min-1172.html> (accessed March 13, 2020).
- 32 B.K. Meyer, A. Polity, D. Reppin, M. Becker, P. Hering, P.J. Klar, T. Sander, C. Reindl, J. Benz, M. Eickhoff, C. Heiliger, M. Heinemann, J. Blasing, A. Krost, S. Shokovets, C. Muller, and C. Running. *Phys. Status Solidi B* **2012**, *249*, 1487.
- 33 L. Zhang, Douglas, A. Blom and H. Wang, *Chem. Meter.* **2011**, *23*, 4587-5498.

- 34 Y. Pan, S. Deng, L. Polavarapu, N. Geo, P. Yuan, C. H. Sow and Q. Xu. *Langmuir* **2012**, 28: 12304
- 35 M.T. Sheldon, P.E. Trudeau, T. Mokari, L.-W. Wang, and A.P. Alivisatos, *Nano let.* **2009**, 9, 6376
- 36 C. Kuo, Y. Yang, S. Gwo, M. Huang, *J Am. Chem. Soc.* **2011**, 133, 1052.
- 37 S. M. Silva, R. Tavallaie, L. Sandiford, R. Tilley, and J. Gooding, *Chem. Commun.* **2016**, 7528.
- 38 H. Wang, K. Yang, S. Hsu, and M. Huang, *Nanoscale*, **2016**, 8, 965.
- 39 Y. Pan, S. Deng, L. Polavarapu, N. Gao, P. Yuan, C. Sow and Q. Xu, *Langmuir*, **2012**, 28, 12304.
40. G.K Paul, Y. Nawa, H. Sato, T. Sakurai, K. Akimoto, *Appl. Phys. Lett.* **2006**, 88, 141901.
41. Scanlon, D. O.; Morgan, B. J.; Watson, G. W.; Walsh, A. *Phys. Rev. Lett.* **2009**, 103, 096405.
42. A.F. Wright, J.S Nelson, *J. Appl. Phys.* **2002**, 92, 5849.
43. Wan-Chen Huang, Lian-Ming Lyu, Yu-Chen Yang, and Michael H. Huang. *Journal of the American Chemical Society* **2012** 134 1261.
44. Jie Wang, Fangling Cui, Sibin Chu, Xiaoquan Jin, Jun Pu, and Zhenghua Wang. *Chempluschem*, **2014**, 79, 684.
45. A. FUJISHIMA and K. HONDA, *Nature*, **1972**, 238, 37.
46. O. Khaselev, J. A. Turner, O. Khaselev and J. A. Turner, *PubMed*, **2012**, 425, 10.
47. M. M. May, H.-J. Lewerenz, D. Lackner, F. Dimroth and T. Hannappel, *Nat. Commun.*, **2015**, 6, 8286.
48. B. Wu and N. Zheng, *Nano Today*, **2013**, 8, 168.
49. M. Szklarczyk and J. O. M. Bockris, *Jouranl Phys. Chem.*, **1984**, 88, 5241.
50. S. Kment, F. Riboni, S. Pausova, L. Wang, L. Wang, H. Han, Z. Hubicka, J. Krysa, P. Schmuki and R. Zboril, *Chem. Soc. Rev.*, **2017**, 46, 3716.

51. A. Paracchino, V. Laporte, K. Sivula, M. Grätzel and E. Thimsen, *Nat. Mater.*, **2011**, *10*, 456.
52. G. Z. Yuan, C. F. Hsia, Z. W. Lin, C. Chiang, Y. W. Chiang and M. H. Huang, *Chem. - A Eur. J.*, **2016**, *22*, 12548.
53. B. Wang, R. Li, Z. Zhang, W. Zhang, X. Yan, X. Wu, G. Cheng and R. Zheng, *J. Mater. Chem. A*, **2017** *34* 567.
54. S. Zhang, R. Jiang, Y. Guo, B. Yang, X. L. Chen, J. Wang and Y. Zhao, *Small*, **2016**, 4264.
55. René Wick and S. David Tilley. *J. Phys. Chem. C*, **2015** *119*,26243-26257
56. L. Xiong, S. Huang, X. Yang, M. Qiu, Z. Chen and Y. Yu. *Electrochimica Acta*.2011, *56*, 2735.
57. G. Garnweitner, M. Niederberger, *J. Am. Ceram. Soc.*, **2006**, *89*, 1801.
58. I. Bilecka, M. Niederberger. *Nanoscale*, **2010**, *2*, 1358.

## Vitae

Name :[MOHAMMED TAJUDEEN ABDULLAHI ]

Nationality :[NIGERIAN ]

Date of Birth :[12/3/1991]

Email :[mtabdullahi01@gmail.com]

Address :[No 12, Shining Rock Street Gauraka, Tafa, LG. Niger St.  
(910103)

Academic Background :[Usmanu Danfodiyo University, Sokoto. ]  
  
(Bachelor Degree in Chemistry, 2013)

[King Fahd University of Petroleum & Minerals. Dhahran, 31261,  
Kingdom of Saudi Arabia. ]  
  
(Master Degree in Chemistry, 2020.)

### Manuscripts:

- Synthesis of Surface Functionalized  $\text{Cu}_2\text{O}$  for Photocatalytic Degradation of ME
- Synthesis, characterization of  $\text{Au@Cu}_2\text{O}$  Hybridized Nanomaterials for PEC water splitting
- Antimicrobial Activity of  $\text{Cu}_2\text{O}$  and  $\text{Au@Cu}_2\text{O}$  Synthesized at Room Temperature